Biased estimates of the isotope ratios of steady-state evaporation from the assumption of equilibrium between vapor and precipitation

Richard P. Fiorella[1], Jason B. West[2], Gabriel J. Bowen[1,3]

1. Department of Geology and Geophysics, University of Utah, Salt Lake City, UT
2. Department of Ecosystem Science and Management, Texas A&M University, College Station, TX
3. Global Change and Sustainability Center, University of Utah, Salt Lake City, UT

Corresponding Author: Rich Fiorella, rich.fiorella@utah.edu, 383 Frederick A Sutton Building, 115 S 1460 E, Salt Lake City, UT 84112

Running Title: Biased estimates of the isotope ratios of steady-state evaporation

Acknowledgements
The authors acknowledge support from National Science Foundation grant EF-1241286. We thank contributors to the SWING2 project for making their model results publicly available.

Keywords
Water isotopes, evaporation, isotopic equilibrium, leaf water, surface waters, climate modeling, water vapor, precipitation

Data availability statement
SWING2 data are hosted by and available from NASA GISS (https://data.giss.nasa.gov/swing2/). ECHAM5 simulations have been made available by N.J. Steiger (http://doi.org/10.5281/zenodo.1249604), while CAM5 data can be obtained from J. Nusbaumer/D.C. Noone.

Abstract

Stable water isotope ratios are measured as a tracer of environmental processes in materials such as leaves, soils, and lakes. Water in these archives may experience evaporation, which increases the abundance of heavy isotopologues in a manner proportional to the gradients in humidity and isotope ratio between the evaporating water and the surrounding atmosphere. Until recently, however, the isotope ratio of the atmosphere has been difficult to measure, and measurements remain scarce. As a result, several assumptions have been adopted to estimate isotope ratios in atmospheric water vapor. Perhaps the most commonly employed assumption in terrestrial environments is that water vapor is in isotopic equilibrium with precipitation. We evaluate this assumption using an 8-member ensemble of general circulation model (GCM) simulations that include explicit calculation of isotope ratios in precipitation and vapor. We find that across the model ensemble water vapor is typically less depleted in heavy isotopologues than expected if it were in equilibrium with annual precipitation. Atmospheric vapor likely possesses higher-than-expected isotope ratios because precipitation isotope ratios are determined by atmospheric conditions that favor condensation, which do not reflect atmospheric mixing and advection processes outside of precipitation events. The effect of this deviation on theoretical estimates of evaporation isotope ratios scales with relative humidity. As a result, the equilibrium assumption gives relatively accurate estimates of the isotope ratios of evaporation in low latitudes, but performs increasingly poorly at increasing latitudes. Future studies of evaporative water pools should include measurements of atmospheric isotope ratios or constrain potential bias with isotope-enabled GCM simulations.

1. Introduction

Phase changes throughout the water cycle drive spatial and temporal variation in water isotope ratios, making these ratios excellent tracers of hydroclimatological and atmospheric processes (Gat, 1996). Variation in precipitation isotope ratios arises from preferential rainout of heavy water isotopologues during condensation, generating spatiotemporal isotopic patterns reflective of atmospheric drivers of advection and condensation across a wide range of scales (Dansgaard, 1964; Rozanski *et al.*, 1993; Bowen and Good, 2015; Bowen *et al.*, 2019). These variations are thought to arise from changes in condensation temperatures (Dansgaard, 1964; Rindsberger *et al.*, 1983; Gat, 1996), precipitation amount (Dansgaard, 1964; Lee and Fung, 2008; Risi *et al.*, 2008) or type (Aggarwal *et al.*, 2016), vapor source (Rindsberger *et al.*, 1983; Liu *et al.*, 2010), upwind precipitation anomalies (e.g., Vimeux *et al.*, 2005; Fiorella *et al.*, 2015), or the residence time of atmospheric water vapor (Aggarwal *et al.*, 2012). As a result, stable isotope ratios are useful for reconstructing hydrological (e.g., Jasechko *et al.*, 2014; Gibson *et al.*, 2016) or ecological (e.g., Bowen *et al.*, 2005; West *et al.*, 2008; Matheny *et al.*, 2017) processes.

Rayleigh distillation is the prevailing model used to understand the evolution of the isotope ratios in precipitation and atmospheric water vapor as water condenses along a transport pathway (Dansgaard, 1964). Rayleigh distillation assumes that liquid water condenses in isotopic equilibrium with the vapor from which it is condensing. Therefore, the change in the isotope ratio of water vapor that has lost mass to condensation can be expressed as:

$$R_v = R_v^0 \left(\frac{q}{q^0}\right)^{\alpha_{eq}-1} \quad \#(1)$$

where R_v is the heavy-to-light isotope ratio in vapor, q is the specific humidity, a superscript 0 refers to conditions prior to any condensation. α_{eq} represents the equilibrium fractionation factor

between liquid and vapor, and is defined by the ratio of isotope ratios in liquid and vapor at equilibrium:

$$\alpha_{eq} = \frac{R_L}{R_V} \#(2)$$

Equilibrium fractionation is temperature dependent (Merlivat and Nief, 1967; Horita and Wesolowski, 1994), and $\alpha_{eq} > 1$ as heavy isotopologues preferentially enter or remain in the liquid or solid phase. Precipitation isotope ratio change due to Rayleigh distillation can be modeled by multiplying both sides of Equation 1 by α_{eq}:

$$R_L = R_v^0 \alpha_{eq} \left(\frac{q}{q^0}\right)^{\alpha_{eq}-1} \#(3)$$

These equations assume that all condensate leaves the air parcel as precipitation, but that air parcel otherwise remains closed, with no additional sources or sinks of moisture. Despite these limiting assumptions, Rayleigh distillation has remained a popular model for explaining variation in water isotope ratios as it successfully captures–at least in trend–large-scale patterns of heavy isotope depletion at high latitudes and elevations, while providing a simple, explicit process linking isotope ratios in precipitation and water vapor.

Many water isotope ratio archives of environmental or paleoenvironmental interest are evaporative systems, such as lakes (e.g., Gibson and Edwards, 2002; Kebede *et al.*, 2009; Gibson *et al.*, 2016), soil waters (Barnes and Allison, 1988; Soderberg *et al.*, 2012), and leaf waters (e.g., Flanagan *et al.*, 1991; Farquhar and Cernusak, 2005; Cernusak *et al.*, 2016), which are subject to post-precipitation enrichment of heavy isotopologues by evaporation. The enrichment of heavy water isotopologues in these pools is typically constrained using the Craig-Gordon model of evaporation (Craig and Gordon, 1965), which predicts the isotope ratio of the evaporating flux

across bulk concentration and isotope ratio gradients between liquid and vapor while accounting for isotopic fractionation:

$$R_E = \alpha_K \frac{\left(\frac{R_L}{\alpha_{eq}} - hR_A\right)}{(1-h)} \#(4)$$

In this equation, R is the heavy-to-light isotope ratio, with subscripts L, E, and A referring to liquid water, the evaporating water flux, and atmospheric water vapor respectively, h representing the ratio in vapor pressures between the observed vapor pressure of the atmosphere and the saturation vapor pressure at the temperature of the liquid surface, and α is the isotopic fractionation factor between liquid and vapor, which describes the magnitude of isotopologues partitioning between the two phases. Subscripts eq and K refer to equilibrium and kinetic fractionation factors respectively. One parameter in this equation, the isotope ratio of atmospheric water vapor, has been difficult to measure at high temporal resolution until recently, and the spatial and temporal scale of these measurements remains limited (Galewsky *et al.*, 2016; Wei *et al.*, 2019). For reconstruction of past environments, isotope ratios of atmospheric water vapor are not available.

In the absence of atmospheric water vapor isotope measurements, it has been suggested that water vapor isotope ratios could be assumed to be in equilibrium with precipitation (Gat, 1996, 2000). The relative abundance of precipitation isotope ratios, which have been measured in locations around the globe for decades, compared to the paucity of long-term vapor isotope ratio measurements, makes this an attractive assumption. However, this assumption has not been widely nor rigorously tested. When posed by Gat (1996, 2000), this assumption was validated by paired vapor-precipitation measurements from a handful of locations, such as Heidelberg, Germany (Jacob and Sonntag, 1991), Krakow, Poland (Schoch-Fischer *et al.*, 1984), and Manaus and Bélem, Brazil (Matsui *et al.*, 1983). In many cases, however, vapor only approached equilibrium with precipitation when data were averaged over multiple years, with significant

seasonal and monthly deviation from equilibrium observed (Schoch-Fischer *et al.*, 1984; Jacob and Sonntag, 1991). More recent high-resolution vapor isotope measurements have further demonstrated that water vapor isotope ratios can be far more dynamic than can be explained by an assumption of equilibrium with monthly or annual precipitation isotope ratios (e.g., Lee *et al.*, 2006; Welp *et al.*, 2008; Noone *et al.*, 2013; Aemisegger *et al.*, 2014; Fiorella *et al.*, 2018). These studies and many others have shown that vapor isotope ratios change in response to a wide variety of processes including air-mass mixing (e.g., Noone *et al.*, 2011), condensation, precipitation, and rainfall evaporation processes (e.g., Lee and Fung, 2008; Risi *et al.*, 2008; Tremoy *et al.*, 2012), evapotranspiration (e.g., Welp *et al.*, 2008; Berkelhammer *et al.*, 2013; Good *et al.*, 2014), and dewfall (e.g., Wen *et al.*, 2012). As a result, it is not clear where, when, and over what timescales this assumption may hold, and its evaluation has been hampered due to a lack of spatially extensive paired vapor and precipitation isotope measurements. Despite these uncertainties, this assumption is often used in isotopic studies of lake water balances (Kebede *et al.*, 2009; Gibson *et al.*, 2016), soil water evaporation (Barnes and Turner, 1998), and leaf water enrichment and transpiration (West *et al.*, 2008; Cernusak *et al.*, 2016).

In the absence of long-term near surface observations of water vapor isotope ratios, we evaluate the assumption of equilibrium between vapor and precipitation globally at monthly to climatological timescales using an ensemble of eight general circulation models that explicitly simulate water vapor and precipitation isotope ratios. We find that the assumption that atmospheric water vapor is nearly in equilibrium with annual precipitation holds best in low latitudes, but performs increasingly worse poleward of 30° latitude, with vapor isotope ratios much higher than would be anticipated were vapor in equilibrium with annual precipitation. At these latitudes, advection of moisture from lower latitudes is required to sustain precipitation

rates, allowing for the possibility for vapor isotope ratios to drift from being in equilibrium with precipitation. In addition, admixture of small amounts of vapor with a high isotope ratio can generate vapor isotope ratios much higher than anticipated via Rayleigh condensation precipitation pathways. As a result, vapor isotope ratios are often decoupled from precipitation isotope ratios via isotopic variation in time and space, where precipitation events only reflect atmospheric conditions during a small fraction of time, and advection supplies isotopically distinct moisture from different source locations.

2. Methods

2.1 Climate model data processing

We generated an ensemble of global climate model simulations (Table 1) that include water isotopes by combining the Stable Water Isotope iNtercomparison Group, version 2 (SWING2; Risi *et al.*, 2012a) simulation archive with more recent global simulations from Nusbaumer et al. (2017) and Steiger et al. (2017). Ocean boundary conditions for all simulations were historical sea surface temperatures (Hurrell *et al.*, 2008; Risi *et al.*, 2012b; Nusbaumer *et al.*, 2017; Steiger *et al.*, 2017). We extracted a common period of 1980-2000 across all simulations. Precipitation isotope ratios were retained where monthly precipitation rates were above 0.1 mm/day, as some models exhibited non-physical isotope ratios at small moisture flux rates. As these situations represent a negligible fraction of precipitation mass, we view them as numerical artifacts that can be dropped from further analysis. Large-scale patterns are not strongly affected by the choice of this threshold, with qualitative differences observed only in the driest regions.

Water isotope tracers are implemented in each model by constructing parallel representations of the hydrological cycle for each major isotopologue (e.g., $^{1}H_{2}^{16}O$, $^{1}H_{2}^{18}O$, and

$^{1}H^{2}H^{16}O$) (Noone and Sturm, 2010). Water isotopologues are treated identically to bulk water during advection processes, and equilibrium and kinetic isotopic fractionations are added to the model physics parameterizations where phase changes occur. The representations of water isotope physics are similar across the model ensemble. Liquid condensate in clouds is assumed to be in isotopic equilibrium with cloud vapor, while vapor deposition onto ice requires more detailed treatment of kinetic isotope effects (e.g., Noone and Sturm, 2010). All models include a representation of evaporation and equilibration of raindrops as they fall through the sub-cloud column. Apart from initial condensation and transit of a raindrop through the sub-cloud model layers, no equilibrium between atmospheric water vapor and precipitation is assumed or prescribed. There are a few differences between water isotope physics across the model ensemble. First, seven of the eight models use kinetic fractionation factors determined by Merlivat (1978), while the HadAM3 model uses kinetic fractionation factors from Cappa et al. (2003). We therefore expect simulated isotope ratios to vary in HadAM3 from the other models where diffusive processes are important, such as in ice clouds at high latitudes (e.g., Jouzel and Merlivat, 1984). Second, each model estimates fractionation and isotopic exchange processes as a raindrop falls through the sub-cloud column, but this process is implemented differently across models. HadAM3, ECHAM5, and MIROC assume that a fixed proportion of water droplets equilibrate with water vapor in the sub-cloud column: 45% of raindrops fully equilibrate for convective clouds (50% in MIROC), while 95% of raindrops fully equilibrate in stratiform clouds (Hoffmann *et al.*, 1998; Werner *et al.*, 2011). In contrast, rain evaporation and sub-cloud equilibration processes are based on Stewart (1975) for the remaining models and provide a more explicit representation of raindrop evaporation and equilibration with the sub-cloud water vapor. Third, calculation of isotope ratios of continental evapotranspiration varies across the models.

Most of the models assume that water returning to the atmosphere is unfractionated relative to soil water, while GISS ModelE and CAM5 explicitly calculate the isotope ratio of evapotranspired water, including fractionation (Aleinov and Schmidt, 2006; Wong *et al.*, 2017). We discuss the potential impacts of these differences in the fluxes from the land model to our results in section 4. Further details of water isotope tracer implementations, as well as descriptions of parameterizations used to simulate the hydrological cycle (e.g., cloud and convective parameterizations), are given in references for each model in Table 1.

Native model resolutions varied from ~1x1° (ECHAM5 and CAM5) to 2.5x3.75° (HadAM3 and LMDZ4) (Table 1). As a result, representation of the land surface and topography were slightly different across models. Water isotope ratios vary strongly with elevation (Siegenthaler and Oeschger, 1980; Rozanski *et al.*, 1993; Bowen and Revenaugh, 2003; Fiorella *et al.*, 2015), and poor representation of surface elevation may bias simulated water isotope ratios, particularly at coarse resolutions. As we are primarily interested in the difference between simulated precipitation and vapor isotope ratios, we expect the impact of this bias to be minimized as it would affect both vapor and precipitation isotope ratios. Coarser resolutions may not be able to resolve small-scale dynamical and transport processes that influence these isotope ratios, however. Simulations were regridded from their native resolution to a common 2x2° grid, which is common practice in multi-model comparisons (e.g., Sanderson *et al.*, 2017). Flux variables were regridded using a second-order conservative method that preserves the global integral (Jones, 1999), while state variables were regridded using bilinear interpolation.

Isotope ratios are expressed in δ notation, where $\delta = 1000(R_x/R_{std}-1)$ and R and R_{std} are the heavy-to-light isotope ratio of a sample x and a standard isotope ratio, respectively. The standard water isotope ratios for $^{18}O/^{16}O$ is 2005.2×10^{-6}, while the standard $^{2}H/^{1}H$ ratio is

155.76 x 10^{-6}, as defined from Vienna Standard Mean Ocean Water (VSMOW) geochemical standard (Coplen, 1996).

2.2 Evaluation of the assumption of equilibrium between precipitation and vapor isotope ratios

To evaluate the assumption of equilibrium between vapor and precipitation, we compare the isotope ratio of water vapor in the lowest model level with vapor in equilibrium with the long-term mean precipitation isotope ratios for each grid cell. This difference can be expressed as:

$$\Delta R_{atm} = R_a - \frac{R_p}{\alpha_{eq}} (5)$$

where R_A and R_P are the isotope ratios of atmospheric vapor and precipitation, respectively, and α_{eq} is the temperature-dependent equilibrium fractionation factor that relates isotope ratios in vapor and liquid (or ice) phases at equilibrium (Equation 2). Where monthly temperatures in the lowest model level were > 0°C, α_{eq} was calculated between liquid and vapor using fractionation factors from Horita and Wesolowski (1994). If temperatures were < 0°C, α_{eq} was calculated between ice and vapor using fractionation factors from Merlivat and Nief (1967). Equation 5 can be expressed in δ notation by substituting $R_{v,e}$, which represents the isotope ratio of vapor in equilibrium with precipitation, for R_p/α_{eq}:

$$\Delta(\delta_{atm}) = \frac{1000\Delta R_{atm}}{R_{std}} = \delta_a - \delta_{v,e} \#(6)$$

We use a Δ(δ) notation to clarify that we are expressing a difference in isotope ratios, which is distinct from the Δ notation for isotopic enrichment that is commonly used in leaf water models (e.g., Cernusak *et al.*, 2016).

For further insight into the processes driving $\Delta(\delta_{atm})$, we compare δ_a and $\delta_{v,e}$ to isotope ratio predictions from air mass mixing and Rayleigh condensation processes. These models predict different responses to isotope ratios with changes in humidity, and define a range of vapor isotope ratios that can be obtained through simple advection, mixing, and condensation processes (Noone, 2012; Bailey *et al.*, 2015; Fiorella *et al.*, 2018). Isotope ratios consistent with Rayleigh distillation are calculated using an initial specific humidity of 28 mmol/mol and an initial δ^2H composition of -80‰. Condensation was modeled by lowering the temperature in 0.5°C steps and calculating the new isotope ratio of the remaining vapor using Rayleigh distillation (Equation 1). This curve describes the evolution of vapor isotope ratios along a trajectory as water is lost to condensation and independent of the conditions promoting condensation. A mixing model was also constructed with end members specified from equatorial and high-latitude specific humidity and isotope ratios derived from the model ensemble. This yielded a dry end member with a specific humidity of 1 mmol/mol and a δ^2H value of -340‰ and a moist end member with a specific humidity of 28 mmol/mol and a δ^2H value of -80‰. Finally, the difference between mixing or Rayleigh model isotope ratio predictions and ensemble average δ_a and $\delta_{v,e}$ values are calculated by subtracting simple isotope model predictions from the GCM ensemble value at the same humidity.

2.3 Calculation of evaporative effects

The Craig-Gordon (1965) model is used to estimate the isotopic composition of evaporating vapor (Equation 4). The evolution of the isotope ratio in an evaporating pool, R_L, can be modeled solving equation 4 for R_L (e.g., Dongmann *et al.*, 1974; Flanagan *et al.*, 1991):

$$R_L = \alpha_{eq}\left[\frac{R_E(1-h)}{\alpha_K} + hR_A\right] \#(7)$$

A second version of equation 7, where R_A is assumed to be in equilibrium with annual precipitation (e.g., $R_A \approx R_{v,e} = R_P/\alpha_{eq}$), can be expressed as:

$$R_L = \alpha_{eq}\left[\frac{R_E(1-h)}{\alpha_K} + \frac{hR_P}{\alpha_{eq}}\right] \#(8)$$

Subtracting equation 8 from equation 7 yields an expression for the bias introduced by this assumption:

$$\Delta R_L = [\alpha_{eq}R_A - R_P]h \#(9)$$

More sophisticated versions of the Craig-Gordon model have been derived for modeling leaf and soil water isotope enrichment (Flanagan *et al.*, 1991; Soderberg *et al.*, 2012), though these models also reduce to equation 9 when a similar difference is calculated.

Using equation 9, and substituting ΔR_{diseq} for $\alpha_{eq}R_A - R_P$, and converting this equation to δ notation yields:

$$\Delta(\delta_L) = \frac{1000}{R_{std}}\Delta R_L = \frac{1000h\Delta R_{diseq}}{R_{std}} = h\Delta(\delta_{diseq}) \#(10)$$

$\Delta(\delta_{diseq})$ can be directly converted to $\Delta(\delta_{atm})$ by dividing by α_{eq}, and the two values represent the same metric but from the perspective of the evaporating water or the atmosphere, respectively.

R_P and R_A are extracted from each model to calculate $\Delta(\delta_L)$, $\Delta(\delta_{diseq})$, and $\Delta(\delta_{atm})$. R_P is calculated for each grid cell as the precipitation amount mass-weighted in $\Delta(\delta_{diseq})$ and $\Delta(\delta_{atm})$ are calculated from 20-year means in the GCM simulations or from monthly R_P values. R_A is extracted from the lowest model level, which is broadly representative of atmospheric boundary layer values. Equilibrium fractionation factors were calculated using the temperature of the lowest model level after Horita and Wesolowski (1994), except for ECHAM5 where 2-m air

temperature was used instead as data from the lowest model level were not archived. We used temperature from the lowest model level instead of surface temperature as the latter quantity was not archived for all models. We calculated $\Delta(\delta_{atm})$ using all combinations of surface, 2-m, and lowest-model-level air temperature available in the archive to determine if this choice impacted our results. The spatial pattern (Fig. S1) and distribution (Fig. S2) of $\Delta(\delta_{atm})$ values exhibited qualitative differences across different temperature sources to calculate α_{eq}, though the differences were small compared to large-scale patterns. Finally, h was estimated using the relative humidity of the lowest model level, as the humidity gradient between saturation specific humidity at the surface and the overlying atmosphere could not be calculated without the surface temperatures. As a result, h may be overestimated where the skin temperature exceeds the air temperature. Finally, GCM-simulated relative humidity values can exhibit supersaturation at high latitudes during winter (Ruosteenoja *et al.*, 2017); we have limited relative humidity values to 100% in the calculation of $\Delta(\delta_L)$.

3. Results

3.1 Spatial patterns of $\Delta(\delta_{atm})$

Several consistent spatial features are observed across the model ensemble. First, values of $\Delta(\delta_{atm}) > 0$, which imply vapor with a higher isotope ratio than predicted by the equilibrium assumption, are more common than $\Delta(\delta_{atm}) < 0$. Second, seven of the GCM simulations have low absolute values of mean annual $\Delta(\delta_{atm})$ in the tropics and subtropics that generally increase away from the equator (Fig. 1). At high latitudes, $\Delta(\delta_{atm})$ can exceed ~8‰ for $\delta^{18}O$ and ~60‰ for $\delta^{2}H$, whereas equatorial $\Delta(\delta_{atm})$ tends toward ~1‰ for $\delta^{18}O$ and ~12‰ for $\delta^{2}H$. The exception to this trend is isoGSM (Fig. 1f), which has a flatter meridional gradient in $\Delta(\delta_{atm})$. The relationship

across the ensemble is strongly linear between $\Delta(\delta^2H_{atm})$ and $\Delta(\delta^{18}O_{atm})$ (Fig. S3), therefore we focus primarily on $\Delta(\delta^2H_{atm})$ moving forward.

Values of $\Delta(\delta^2H_{atm})$ are most positive over land in sub-Saharan Africa, East Asia, East India, northern North America, and most of South America, whereas the most positive values of $\Delta(\delta^2H_{atm})$ over the ocean are observed where there is perennial or seasonal sea ice (Fig. 1). HadAM3 exhibits a distinct response in the northern high latitudes, however, as the only model that suggests negative $\Delta(\delta_{atm})$ values in this region (Fig. 1f). The negative $\Delta(\delta_{atm})$ values observed in HadAM3 at high latitudes is likely due to this model's use of diffusive fractionation factors from Cappa et al. (2003), while the remainder of the models use fractionation factors determined by Merlivat (1978). In addition, HadAM3 has the highest supersaturation parameter, which describes the increase of supersaturation with decreases in temperature, of any model in this study (Pope *et al.*, 2000; Tindall *et al.*, 2009), increasing the importance of diffusive processes at cold temperatures and high latitudes (e.g., Jouzel and Merlivat, 1984) for this model. Negative $\Delta(\delta_{atm})$ values are observed across the model ensemble in the Sahara, the Middle East, and East Antarctica over land, and under the subtropical highs over the ocean (Fig. 1).

Responses differ in sign across models for northeastern Siberia, West Antarctica, Australia, Greenland, and the southwestern United States. In particular, Antarctic values of $\Delta(\delta_{atm})$ vary dramatically across models, with the ensemble standard deviation usually exceeding 40‰ for δ^2H (Fig. 1j). Given the low evaporation rates and cold temperatures over Antarctica, and the strong sensitivity of water isotope ratios to parameterizations of ice supersaturation (Jouzel and Merlivat, 1984), which likely vary across the model ensemble, we exclude values over Antarctica from further analysis. Over Siberia, values of $\Delta(\delta_{atm})$ are weakly positive for CAM2, GISS ModelE, and MIROC (Fig. 1a,d,h), positive for CAM5 (Fig. 1b), and negative for

ECHAM5, HadAM3, isoGSM, and LMDZ (Fig. 1c,e,f,g). High intermodal spread in this region may also be due to parameterizations of isotopic fractionation under cold conditions. In contrast, over Australia and the southwestern United States, absolute values of $\Delta(\delta^2H_{atm})$ and its variance across the model ensemble tend to be low (Fig. 1).

Seasonal patterns in $\Delta(\delta^2H_{atm})$ show large-scale consistency in trend (Fig. 2), with the exception of high-latitude winter. Highly positive values of $\Delta(\delta^2H_{atm})$ are found in the southern ocean for all seasons (Fig. 2). During boreal winter / austral summer (DJF), high-latitude $\Delta(\delta^2H_{atm})$ values are generally greater than 0 (Fig. 2a), except for HadAM3, which predicts $\Delta(\delta^2H_{atm})$ values much less than zero and is likely a result of HadAM3's use of the Cappa et al. (2003) kinetic fractionation factors. DJF ensemble mean $\Delta(\delta^2H_{atm})$ are ~10‰ between 30° and 30°S (Fig. 2a), and gradually increase between 30° and 60° latitude in both hemispheres. When ocean grid cells are excluded, ECHAM5 and LMDZ also predict $\Delta(\delta^2H_{atm})$ values below 0 at high northern latitudes, and $\Delta(\delta^2H_{atm})$ values between 60°S and 60°N are more variable (Fig. 2b). During boreal summer / austral winter (JJA), ensemble mean $\Delta(\delta^2H_{atm})$ values are near zero in the northern hemisphere subtropics, and generally increase moving away from these latitudes, with a small local minimum in the southern hemisphere midlatitudes (Fig. 2c). Similar patterns for JJA are observed when $\Delta(\delta^2H_{atm})$ is calculated using land cells only, though the local minimum in the southern hemisphere midlatitudes is more pronounced, and the northern hemisphere subtropical minimum in $\Delta(\delta^2H_{atm})$ values is less than 0 (Fig. 2d), likely a result of negative values throughout the Sahara desert (Fig. 1). These seasonal patterns demonstrate in summer, when evaporative fluxes are highest, $\Delta(\delta^2H_{atm})$ values are generally positive outside of the northern hemisphere subtropics.

These patterns observed in the ensemble do not seem to be sensitive to the timescales over which long-term averages of $\Delta(\delta^2H_{atm})$ are calculated. For example, restricting calculation of $\Delta(\delta^2H_{atm})$ to months where the mean temperature was above zero (e.g., following West et al., 2008) does not reduce values of $\Delta(\delta^2H_{atm})$ (Fig. S4). Similarly, weighting values of $\Delta(\delta^2H_{atm})$ by monthly evaporation (Fig. S5) or precipitation (Fig. S6) fluxes has little impact or even increases values of $\Delta(\delta^2H_{atm})$ (Fig. S7). Therefore, we retain the annual average values for the remainder of the analysis.

For each model, >75% of all grid cells have $\Delta(\delta^2H_{atm})$ and $\Delta(\delta^{18}O_{atm}) > 0$ when Antarctica is excluded (Fig. 2ab). CAM5 has the highest median $\Delta(\delta_{atm})$ values, while LMDZ has the lowest (Fig. 2ab). CAM5 $\Delta(\delta_{atm})$ values are nearly universally positive, with >97% of all grid cells having $\Delta(\delta^2H_{atm})$ and $\Delta(\delta^{18}O_{atm}) > 0$. When ocean cells are also excluded, median values of $\Delta(\delta^2H_{atm})$ and $\Delta(\delta^{18}O_{atm})$ are not meaningfully changed, but the distribution shifts from tending to have a long tail of highly positive $\Delta(\delta_{atm})$ values to being more centered (Fig. 2cd), with the exception of HadAM3. However, despite changes in the distributions when ocean cells are excluded, >75% of land grid cells still exhibit $\Delta(\delta_{atm})$ values > 0.

3.2. Atmospheric moisture balance and transport govern $\Delta(\delta_{atm})$ values

Patterns in $\Delta(\delta_{atm})$ can be related to fundamental features of the balance of precipitation to evaporation, atmospheric circulation and moisture transport. Simulation of precipitation minus evaporation, or P-E, was similar between all model simulations (Fig. S8). Large differences in P-E were only observed in the deep tropics, where the position of the Intertropical Convergence Zone varied between simulations, perhaps due to in part to variations in model resolution. Values of $\Delta(\delta^2H_{atm}) < 0$ tended to occur in regions where precipitation and evaporation rates were both

low and near equal to each other (Fig. 4a) in regions of atmospheric subsidence (Fig. 4b). In these regions, atmospheric vapor is lighter than would be expected from an assumption of equilibrium with precipitation, likely reflecting the admixture of dry air in the descending limb of the Hadley cell. Subtropical deserts, which are associated with large-scale atmospheric subsidence, indeed tend to have $\Delta(\delta^2H_{atm}) < 0$ across all of the model simulations (Fig. 1). Negative $\Delta(\delta^2H_{atm})$ values over land tend to be more negative than over the ocean, perhaps due to lower local evaporative fluxes over land than over the ocean in these regions. In contrast, regions where precipitation exceeds evaporation tend to have $\Delta(\delta^2H_{atm}) > 0$ (Fig. 4ac), and also have vertical pressure velocities either close to zero or indicative of ascent (Fig.4b). Two distinct patterns associated with $\Delta(\delta^2H_{atm}) > 0$ are observed: tropical regions with high precipitation rates, and mid- and high-latitude regions with moderate precipitation rates. A common feature of mid- and high-latitude sites with high $\Delta(\delta^2H_{atm})$ is that they tend to be regions where precipitation vastly outweighs evaporation, indicating that moisture must be advected into these regions to sustain these precipitation rates. Regions where atmospheric vapor is nearly in equilibrium with annual precipitation tend to be regions where evaporation is much higher than precipitation (Fig. 4ac), and precipitation rates are low (Fig. 4c).

These patterns can be unified by considering atmospheric processes underlying the water budget of these different hydroclimatic regimes, as humidity changes associated with condensation and meridional mixing should produce distinct changes in isotope ratios (Fig. 5ab). Water vapor δ^2H values simulated by the GCMs cluster close to the mass-balance model (following Noone, 2012) predictions for atmospheric mixing (Fig. 5a). In contrast, vapor in equilibrium with modeled annual precipitation clusters close to the Rayleigh condensation model prediction at low and high humidities and traces an intermediate path between mixing and

Rayleigh end members in between (Fig. 5b). As a result, the mixing model captures trends in modeled atmospheric vapor quite well, while it tends to overestimate isotope ratios of vapor in equilibrium with precipitation (Fig. 5c). Likewise, the Rayleigh model tends to underestimate isotope ratios for modeled vapor and vapor in equilibrium with precipitation, but the magnitude of the underestimation of the latter is less than the former (Fig. 5c).

These trends likely arise for two reasons. First, precipitation reflects atmospheric conditions that favor condensation by definition. Precipitation only occurs over land ~8% of the time, and the fraction of the time it rains is below 50% even in the rainiest locations (Trenberth and Zhang, 2018). Therefore, even if precipitation is in equilibrium with vapor where and when it occurs, precipitation represents only a subset of atmospheric conditions that is by nature biased toward the Rayleigh model. Second, the shape of the mixing relationship suggests that atmospheric isotope ratios change little across large ranges in humidity when sufficiently wet, and are always greater than those predicted by Rayleigh distillation. As a result, small additions of vapor with comparatively high isotope ratios at times when precipitation is not occurring can cause strong positive deviations from the Rayleigh curve. Additionally, the space between the Rayleigh and mixing curves is small at high humidities, but grows as humidity decreases. At high humidities, isotope ratios predicted from air-mass mixing or Rayleigh condensation are similar, and the transition from one process to the other cannot have a large impact on isotope ratios without a large change in humidity. We suspect this factor is the origin of small magnitude values of $\Delta(\delta^2H_{atm})$ are observed in the deep tropics (Fig. 1) despite high precipitation relative to local evaporation (Fig. 4, S8). In contrast, at the lower humidities characteristic of the mid- and high-latitudes, the isotope ratio range between Rayleigh and mixing model predictions is large (Fig. 5). Large positive $\Delta(\delta^2H_{atm})$ values over humid land areas and over seasonal sea ice likely

(Fig. 1) arise from the tendency of vapor isotope ratios to be higher under large-scale air-mass mixing than during condensation processes.

3.3. Impact of $\Delta(\delta_{atm})$ on isotope ratios of evaporating water pools

If these model-simulated differences between vapor δ^2H values and precipitation-equilibrated vapor values are reflective of the real world, however, their impact on theoretical estimates of the isotopic composition of evaporation also scales with relative humidity (Eqn. 10). We analyze this impact for grid cells corresponding to land, where such estimates are widely used to interpret data from lakes, leaf waters, and soils. We multiply $\Delta(\delta_{atm})$ values by α_{eq} to yield $\Delta(\delta_{diseq})$, and then scale these values by relative humidity to obtain $\Delta(\delta_L)$. Since α_{eq} is greater than–but close to–1, the absolute values of $\Delta(\delta_{diseq})$ are similar to but larger than the absolute values of $\Delta(\delta_{atm})$. Due to α_{eq} increasing with decreasing temperatures, however, this transformation does increase the equator-to-pole gradient slightly (Fig 5a). As mean relative humidity is generally below 100% (Fig. 6b), $\Delta(\delta_L)$ is lower than $\Delta(\delta_{diseq})$ at all latitudes (Fig. 6c), but particularly in the subtropics where relative humidities are ≤ 50% on average (Fig. 6b). Equatorward of 30°, $\Delta(\delta^2H_L)$ values are small (typically < 10‰, Fig. 6c), as $\Delta(\delta_{diseq})$ is low in the deep tropics (Fig. 6a) while relative humidity is low in the subtropics (Fig. 6b). At these latitudes, the assumption that vapor is in equilibrium with precipitation may be useful. Poleward of ~45°, however, relative humidity and $\Delta(\delta_{diseq})$ both increase, yielding Δ^2H_L values that exceed ~20‰ at many latitudes (Fig. 6c). At these latitudes, adopting an assumption of equilibrium between vapor and precipitation is likely to introduce substantial bias in the interpretation of water isotope ratio data.

4. Discussion

The assumption that atmospheric water vapor isotope ratios are in equilibrium with local annual precipitation isotope ratios rarely holds across an ensemble of isotope-enabled GCMs. We find a broadly consistent pattern across GCMs where atmospheric vapor usually has a higher heavy isotopologue content than anticipated for atmospheric vapor in isotopic equilibrium with annual precipitation. As a result, Craig-Gordon calculations are prone to underestimate the isotope ratio of evaporating waters in most places when adopting this assumption. Exceptions to this trend include regions of persistent atmospheric subsidence, where admixture of highly distilled vapor in descending air nudge water vapor isotope ratios to be lower than $\delta_{v,e}$, and regions where evaporation far exceeds precipitation, where δ_v approaches $\delta_{v,e}$. The deviations of isotope ratios from the Craig-Gordon model predictions described here are distinct from a different source of deviations commonly described in leaf water studies. Several studies in leaf waters have shown a tendency of the Craig-Gordon model to overestimate leaf water enrichment, as leaf waters frequently possess isotope ratios that are lower than predicted isotope ratios (e.g., Flanagan *et al.*, 1991; Cernusak *et al.*, 2016). Our results using GCMs here suggest that assuming δ_v and $\delta_{v,e}$ are equal may partially mask this effect, as Craig-Gordon-modeled isotope ratios would be even higher for leaf waters were δ_v used in place of $\delta_{v,e}$. Finally, we have characterized these trends using isotope ratios in GCMs as paired vapor and precipitation isotope records remain rare. However, new large-scale observational networks such as the National Ecological Observatory Network (Thorpe *et al.*, 2016), or improved processing of satellite observations of water vapor isotope ratios to yield better estimates of near-surface vapor isotope ratios (e.g., Worden *et al.*, 2012), will allow broad testing and validation of our results.

4.1. Over what timescales is precipitation in equilibrium with atmospheric water vapor?

Decoupling of δ_v from $\delta_{v,e}$ occurs across both time and space due to the relative rarity of precipitation with respect to moisture advection in the atmosphere. Precipitation selects for a particular set of atmospheric conditions that favor condensation or ice nucleation. Equilibrium between atmospheric water vapor and precipitation is commonly observed for sufficiently long precipitation events (e.g., Stewart, 1975; Lee and Fung, 2008), yet in order for δ_v to remain coupled to $\delta_{v,e}$ this relationship must persist after precipitation ends. In fact, many studies (e.g., Lee *et al.*, 2006; Angert *et al.*, 2008; Welp *et al.*, 2008; Griffis *et al.*, 2016) have shown substantial deviations from the equilibrium assumption when precipitation and vapor are compared at monthly timescales. Furthermore, rapid changes in vapor isotope ratios are apparent with weather events such as frontal passages (e.g., Lee *et al.*, 2006; Aemisegger *et al.*, 2015; Fiorella *et al.*, 2018), and large diurnal variability driven by evapotranspiration and boundary layer mixing is commonly observed in high-resolution vapor isotope records (e.g., Lai and Ehleringer, 2011; Welp *et al.*, 2012; Fiorella *et al.*, 2018). Differences emerge between δ_v and $\delta_{v,e}$ therefore, because precipitation is a relatively rare occurrence and other processes with distinct isotopic effects may dominate the atmospheric water budget during periods of non-precipitation. In particular, even slight moistening by mixing with moist air that has not experienced substantial condensation can push δ_v to much higher values than would be consistent with Rayleigh condensation. Isotope ratios predicted by simple mixing and Rayleigh models converge at the humidity extremes, but diverge quite substantially at intermediate humidity values (Fig. 5). As mixing and/or advection contribute to atmospheric re-moistening during periods between precipitation events, this will systematically push vapor values away from precipitation-equilibrium values, as observed in most regions here.

Precipitation could be in equilibrium with vapor at shorter time scales but out of equilibrium when averaged at annual timescales. However, changing the basis of comparison from annual precipitation isotope ratios to the current month's precipitation isotope ratios does not meaningfully change the distribution of $\Delta(\delta_{atm})$ (Fig. 7). Persistence of this bias when using monthly modeled precipitation isotope ratios indicates that precipitation timing and moisture advection processes continuously promote decoupling of δ_v from $\delta_{v,e}$. Furthermore, it suggests that this bias is not primarily driven by seasonal changes in moisture source or precipitation type. Gat (2000) noted that equilibrium between δ_v and $\delta_{v,e}$ is often inhibited for snow or ice hydrometeors, as isotopic exchange between these hydrometeors and the atmospheric column they fall through is attenuated. Our results suggest that processes promoting differences between δ_v and $\delta_{v,e}$ are more fundamental, and occur throughout the year and at all latitudes.

5. Conclusions

Modeling the evaporative enrichment of heavy isotopologues in evaporating water pools, such as leaves, lakes, and soils, has relied on the Craig-Gordon model and requires knowledge or assumptions about the isotope ratios in atmospheric water vapor. Until recently, measurements of the isotope ratio of atmospheric water vapor have been labor intensive and difficult to obtain, leading to assumptions about how to estimate the isotope ratio of atmospheric water. We show that the assumption that atmospheric vapor is in equilibrium with annual precipitation isotope ratios (Gat, 1996, 2000) is rarely valid using an ensemble of GCM simulations that include explicit modeling of vapor and precipitation isotope ratios. Atmospheric vapor is typically less depleted in heavy isotopologues than would be expected were it in equilibrium with annual precipitation, and is most prominent in regions where advection and moisture convergence are

the dominant sources of water vapor and precipitation instead of evaporation. The magnitude of this deviation from equilibrium generally increases from equator to pole. Vapor isotope ratios in equilibrium with precipitation are nudged toward predictions from a Rayleigh condensation model, while modeled vapor isotope ratios are better described by a simple equator-to-pole atmospheric mixing model. This result suggests that adopting an assumption of equilibrium between vapor and precipitation in using the Craig-Gordon model overvalues the role of precipitation in setting vapor isotope ratios, as precipitation reflects only a subset of atmospheric conditions that promote their variability. The salient exception to this trend occurs where large-scale atmospheric subsidence dominates, producing vapor isotope ratios that are more depleted in heavy isotopologues than expected from an assumption of equilibrium between vapor and precipitation due to the admixture of heavily-distilled water vapor transported in the subsiding air.

The impact of deviation in atmospheric vapor isotope ratios from equilibrium with precipitation on evaporating water pools, however, depends on the humidity gradient between the atmosphere and the evaporating water. For latitudes equatorward of ~30°, the combination of lower relative humidities and/or comparatively small $\Delta(\delta_{atm})$ values result in small values of $\Delta(\delta_L)$. In these cases, the assumption that atmospheric vapor is in equilibrium with precipitation may hold sufficiently well. Poleward of ~30°, however, adopting the assumption that $\Delta(\delta_{atm})$ is near zero will produce estimates of the isotope ratio of atmospheric water vapor that are biased to have too low of a heavy isotopologue content. This pattern is reinforced by higher mean relative humidity values. To account for these systematic biases, future studies should incorporate measurements of the isotope ratio of atmospheric water vapor or, particularly for paleoenvironmental reconstructions, consider using constraints from an isotope-enabled GCM.

529

References

Aemisegger F, Pfahl S, Sodemann H, Lehner I, Seneviratne SI, Wernli H. 2014. Deuterium excess as a proxy for continental moisture recycling and plant transpiration. *Atmospheric Chemistry and Physics* **14** (8): 4029–4054 DOI: 10.5194/acp-14-4029-2014

Aemisegger F, Spiegel JK, Pfahl S, Sodemann H, Eugster W, Wernli H. 2015. Isotope meteorology of cold front passages: A case study combining observations and modeling. *Geophysical Research Letters* **42** (13): 5652–5660 DOI: 10.1002/2015GL063988

Aggarwal PK, Alduchov OA, Froehlich KO, Araguas-Araguas LJ, Sturchio NC, Kurita N. 2012. Stable isotopes in global precipitation: A unified interpretation based on atmospheric moisture residence time. *Geophysical Research Letters* **39** (11): n/a-n/a DOI: 10.1029/2012GL051937

Aggarwal PK, Romatschke U, Araguas-Araguas L, Belachew D, Longstaffe FJ, Berg P, Schumacher C, Funk A. 2016. Proportions of convective and stratiform precipitation revealed in water isotope ratios. *Nature Geoscience* **9** (8): 624–629 DOI: 10.1038/ngeo2739

Aleinov I, Schmidt GA. 2006. Water isotopes in the Giss ModelE land surface scheme. *Global and Planetary Change* **51**: 108–120

Angert A, Lee J-E, Yakir D. 2008. Seasonal variations in the isotopic composition of near-surface water vapour in the eastern Mediterranean. *Tellus B: Chemical and Physical Meteorology* **60** (4): 674–684 DOI: 10.1111/j.1600-0889.2008.00357.x

Bailey A, Nusbaumer J, Noone D. 2015. Precipitation efficiency derived from isotope ratios in water vapor distinguishes dynamical and microphysical influences on subtropical atmospheric constituents. *Journal of Geophysical Research: Atmospheres* **120** (18): 9119–9137 DOI: 10.1002/2015JD023403

Barnes CJ, Allison GB. 1988. Tracing of water movement in the unsaturated zone using stable isotopes of hydrogen and oxygen. *Journal of Hydrology* **100** (1–3): 143–176 DOI: 10.1016/0022-1694(88)90184-9

Barnes CJ, Turner JV. 1998. Isotopic Exchange in Soil Water. In *Isotope Tracers in Catchment Hydrology*Elsevier; 137–163. DOI: 10.1016/B978-0-444-81546-0.50012-4

Berkelhammer M, Hu J, Bailey A, Noone DC, Still CJ, Barnard H, Gochis D, Hsiao GS, Rahn T, Turnipseed A. 2013. The nocturnal water cycle in an open-canopy forest. *Journal of Geophysical Research: Atmospheres* **118** (17): 10,225-10,242 DOI: 10.1002/jgrd.50701

Bowen GJ, Good SP. 2015. Incorporating water isoscapes in hydrological and water resource investigations: Isoscapes in hydrological and water resource investigations. *Wiley Interdisciplinary Reviews: Water* **2** (2): 107–119 DOI: 10.1002/wat2.1069

Bowen GJ, Revenaugh J. 2003. Interpolating the isotopic composition of modern meteoric precipitation. *Water Resources Research* **39** (10) DOI: 10.1029/2003WR002086

Bowen GJ, Cai Z, Fiorella RP, Putman AL. 2019. Isotopes in the Water Cycle: Regional- to Global-Scale Patterns and Applications. *Annual Review of Earth and Planetary Sciences* **47**: 27 DOI: 10.1146/annurev-earth-053018-060220

Bowen GJ, Wassenaar LI, Hobson KA. 2005. Global application of stable hydrogen and oxygen isotopes to wildlife forensics. *Oecologia* **143** (3): 337–348 DOI: 10.1007/s00442-004-1813-y

Cappa CD, Hendricks MB, DePaolo DJ, Cohen RC. 2003. Isotopic fractionation of water during evaporation. *Journal of Geophysical Research* **108** (D16) DOI: 10.1029/2003JD003597

Cernusak LA, Barbour MM, Arndt SK, Cheesman AW, English NB, Feild TS, Helliker BR, Holloway-Phillips MM, Holtum JAM, Kahmen A, et al. 2016. Stable isotopes in leaf water of terrestrial plants. *Plant, Cell & Environment* **39** (5): 1087–1102 DOI: 10.1111/pce.12703

Collins WD, Hack JJ, Boville BA, Rasch PJ, Williamson DL, Kiehl JT, Briegleb B, McCaa JR, Bitz CM, Lin S-J, et al. 2002. Description of the NCAR Community Atmosphere Model (CAM2). NCAR Technical Note.

Coplen TB. 1996. New guidelines for reporting stable hydrogen, carbon, and oxygen isotope-ratio data. *Geochimica et Cosmochimica Acta* **60** (17): 3359–3360 DOI: 10.1016/0016-7037(96)00263-3

Craig H, Gordon LI. 1965. Deuterium and oxygen-18 variations in the ocean and the marine atmosphere. In *Stable Isotopes in Oceanographic Studies and Paleotemperatures*.

Dansgaard W. 1964. Stable isotopes in precipitation. *Tellus* **16** (4): 436–468 DOI: 10.1111/j.2153-3490.1964.tb00181.x

Dongmann G, Nürnberg HW, Förstel H, Wagener K. 1974. On the enrichment of $H_2{}^{18}O$ in the leaves of transpiring plants. *Radiation and environmental biophysics* **11** (1): 41–52

Farquhar GD, Cernusak LA. 2005. On the isotopic composition of leaf water in the non-steady state. *Functional Plant Biology* **32** (4): 293 DOI: 10.1071/FP04232

Fiorella RP, Poulsen CJ, Matheny AM. 2018. Seasonal Patterns of Water Cycling in a Deep, Continental Mountain Valley Inferred From Stable Water Vapor Isotopes. *Journal of Geophysical Research: Atmospheres* DOI: 10.1029/2017JD028093

Fiorella RP, Poulsen CJ, Pillco Zolá RS, Barnes JB, Tabor CR, Ehlers TA. 2015. Spatiotemporal variability of modern precipitation $\delta^{18}O$ in the central Andes and implications for paleoclimate and paleoaltimetry estimates. *Journal of Geophysical Research: Atmospheres* **120** (10): 4630–4656 DOI: 10.1002/2014JD022893

Flanagan LB, Comstock JP, Ehleringer JR. 1991. Comparison of Modeled and Observed Environmental Influences on the Stable Oxygen and Hydrogen Isotope Composition of Leaf Water in Phaseolus vulgaris L. *Plant Physiology* **96** (2): 588–596 DOI: 10.1104/pp.96.2.588

Galewsky J, Steen-Larsen HC, Field RD, Worden J, Risi C, Schneider M. 2016. Stable isotopes in atmospheric water vapor and applications to the hydrologic cycle. *Reviews of Geophysics* **54** (4): 809–865 DOI: 10.1002/2015RG000512

Gat JR. 1996. Oxygen and hydrogen isotopes in the hydrologic cycle. *Annual Review of Earth and Planetary Sciences* **24**: 225–62

Gat JR. 2000. Atmospheric water balance: the isotopic perspective. *Hydrological Processes* **14** (8): 1357–1369 DOI: 10.1002/1099-1085(20000615)14:8<1357::AID-HYP986>3.0.CO;2-7

Gibson JJ, Edwards TWD. 2002. Regional water balance trends and evaporation-transpiration partitioning from a stable isotope survey of lakes in northern Canada. *Global Biogeochemical Cycles* **16** (2): 10-1-10–14 DOI: 10.1029/2001GB001839

Gibson JJ, Birks SJ, Yi Y. 2016. Stable isotope mass balance of lakes: a contemporary perspective. *Quaternary Science Reviews* **131**: 316–328 DOI: 10.1016/j.quascirev.2015.04.013

Good SP, Soderberg K, Guan K, King EG, Scanlon TM, Caylor KK. 2014. δ^2H isotopic flux partitioning of evapotranspiration over a grass field following a water pulse and subsequent dry down. *Water Resources Research* **50** (2): 1410–1432 DOI: 10.1002/2013WR014333

Griffis TJ, Wood JD, Baker JM, Lee X, Xiao K, Chen Z, Welp LR, Schultz NM, Gorski G, Chen M, et al. 2016. Investigating the source, transport, and isotope composition of water vapor in the planetary boundary layer. *Atmospheric Chemistry and Physics* **16** (8): 5139–5157 DOI: 10.5194/acp-16-5139-2016

Hoffmann G, Werner M, Heimann M. 1998. Water isotope module of the ECHAM atmospheric general circulation model: A study on timescales from days to several years. *Journal of Geophysical Research: Atmospheres* **103** (D14): 16871–16896 DOI: 10.1029/98JD00423

Horita J, Wesolowski DJ. 1994. Liquid-vapor fractionation of oxygen and hydrogen isotopes of water from the freezing to the critical temperature. *Geochimica et Cosmochimica Acta* **58** (16): 3425–3437 DOI: 10.1016/0016-7037(94)90096-5

Hourdin F, Musat I, Bony S, Braconnot P, Codron F, Dufresne J-L, Fairhead L, Filiberti M-A, Friedlingstein P, Grandpeix J-Y, et al. 2006. The LMDZ4 general circulation model: climate performance and sensitivity to parametrized physics with emphasis on tropical convection. *Climate Dynamics* **27** (7–8): 787–813 DOI: 10.1007/s00382-006-0158-0

Hurrell JW, Hack JJ, Shea D, Caron JM, Rosinski J. 2008. A New Sea Surface Temperature and Sea Ice Boundary Dataset for the Community Atmosphere Model. *Journal of Climate* **21** (19): 5145–5153 DOI: 10.1175/2008JCLI2292.1

Jacob H, Sonntag C. 1991. An 8-year record of the seasonal variation of ^{2}H and ^{18}O in atmospheric water vapour and precipitation at Heidelberg, Germany. *Tellus* **43B**: 291–300

Jasechko S, Birks SJ, Gleeson T, Wada Y, Fawcett PJ, Sharp ZD, McDonnell JJ, Welker JM. 2014. The pronounced seasonality of global groundwater recharge. *Water Resources Research* **50** (11): 8845–8867 DOI: 10.1002/2014WR015809

Jones PW. 1999. First- and Second-Order Conservative Remapping Schemes for Grids in Spherical Coordinates. *Monthly Weather Review* **127** (9): 2204–2210 DOI: 10.1175/1520-0493(1999)127<2204:FASOCR>2.0.CO;2

Jouzel J, Merlivat L. 1984. Deuterium and oxygen 18 in precipitation: Modeling of the isotopic effects during snow formation. *Journal of Geophysical Research* **89** (D7): 11749 DOI: 10.1029/JD089iD07p11749

K-1 model developers. K-1 Coupled GCM (MIROC) Description. Center for Climate System Research, University of Tokyo; National Institute for Environmental Studies; Frontier Research Center for Global Change.

Kanamitsu M, Kumar A, Juang H-MH, Schemm J-K, Wang W, Yang F, Hong S-Y, Peng P, Chen W, Moorthi S, et al. 2002. NCEP Dynamical Seasonal Forecast System 2000. *Bulletin of the American Meteorological Society* **83** (7): 1019–1037 DOI: 10.1175/1520-0477(2002)083<1019:NDSFS>2.3.CO;2

Kebede S, Travi Y, Rozanski K. 2009. The δ^{18}O and δ^2H enrichment of Ethiopian lakes. *Journal of Hydrology* **365** (3–4): 173–182 DOI: 10.1016/j.jhydrol.2008.11.027

Kurita N, Noone D, Risi C, Schmidt GA, Yamada H, Yoneyama K. 2011. Intraseasonal isotopic variation associated with the Madden-Julian Oscillation. *Journal of Geophysical Research: Atmospheres* **116** (D24): n/a-n/a DOI: 10.1029/2010JD015209

Lai C-T, Ehleringer JR. 2011. Deuterium excess reveals diurnal sources of water vapor in forest air. *Oecologia* **165** (1): 213–223 DOI: 10.1007/s00442-010-1721-2

Lee J-E, Fung I. 2008. "Amount effect" of water isotopes and quantitative analysis of post-condensation processes. *Hydrological Processes* **22** (1): 1–8 DOI: 10.1002/hyp.6637

Lee J-E, Fung I, DePaolo DJ, Henning CC. 2007. Analysis of the global distribution of water isotopes using the NCAR atmospheric general circulation model. *Journal of Geophysical Research* **112** (D16) DOI: 10.1029/2006JD007657

Lee X, Smith R, Williams J. 2006. Water vapour $^{18}O/^{16}O$ isotope ratio in surface air in New England, USA. *Tellus B: Chemical and Physical Meteorology* **58** (4): 293–304 DOI: 10.1111/j.1600-0889.2006.00191.x

Liu Z, Bowen GJ, Welker JM. 2010. Atmospheric circulation is reflected in precipitation isotope gradients over the conterminous United States. *Journal of Geophysical Research* **115** (D22) DOI: 10.1029/2010JD014175

Matheny AM, Fiorella RP, Bohrer G, Poulsen CJ, Morin TH, Wunderlich A, Vogel CS, Curtis PS. 2017. Contrasting strategies of hydraulic control in two codominant temperate tree species. *Ecohydrology* **10** (3): e1815 DOI: 10.1002/eco.1815

Matsui E, Salati E, Ribeiro MNG, Reis CM, Tancredi ACSNF, Gat JR. 1983. Precipitation in the central Amazon Basin: - The isotopic composition of rain and atmospheric moisture at Belém and Manaus. *Acta Amazonica* **13** (2): 307–369 DOI: 10.1590/1809-43921983132307

Merlivat L. 1978. Molecular diffusivities of $H_2{}^{16}O$, $HD^{16}O$, and $H_2{}^{18}O$ in gases. *The Journal of Chemical Physics* **69** (6): 2864 DOI: 10.1063/1.436884

Merlivat L, Nief G. 1967. Fractionnement isotopique lors des changements d'état solide-vapeur et liquide-vapeur de l'eau à des températures inférieures à 0°C. *Tellus* **19** (1): 122–127 DOI: 10.1111/j.2153-3490.1967.tb01465.x

Neale RB, Gettelman A, Park S, Chen C-C, Lauritzen PH, Williamson DL, Conley AJ, Kinnison D, Marsh D, Smith AK, et al. 2010. Description of the NCAR Community Atmosphere Model (CAM 5.0). NCAR/TN-486+STR. NCAR.

Noone D. 2012. Pairing Measurements of the Water Vapor Isotope Ratio with Humidity to Deduce Atmospheric Moistening and Dehydration in the Tropical Midtroposphere. *Journal of Climate* **25** (13): 4476–4494 DOI: 10.1175/JCLI-D-11-00582.1

Noone D, Sturm C. 2010. Comprehensive Dynamical Models of Global and Regional Water Isotope Distributions. In *Isoscapes*, West JB, , Bowen GJ, , Dawson TE, , Tu KP (eds).Springer Netherlands: Dordrecht; 195–219. DOI: 10.1007/978-90-481-3354-3_10

Noone D, Galewsky J, Sharp ZD, Worden J, Barnes J, Baer D, Bailey A, Brown DP, Christensen L, Crosson E, et al. 2011. Properties of air mass mixing and humidity in the subtropics from measurements of the D/H isotope ratio of water vapor at the Mauna Loa Observatory. *Journal of Geophysical Research: Atmospheres* **116** (D22): n/a-n/a DOI: 10.1029/2011JD015773

Noone D, Risi C, Bailey A, Berkelhammer M, Brown DP, Buenning N, Gregory S, Nusbaumer J, Schneider D, Sykes J, et al. 2013. Determining water sources in the boundary layer from tall tower profiles of water vapor and surface water isotope ratios after a snowstorm in Colorado. *Atmospheric Chemistry and Physics* **13** (3): 1607–1623 DOI: 10.5194/acp-13-1607-2013

Nusbaumer J, Wong TE, Bardeen C, Noone D. 2017. Evaluating hydrological processes in the Community Atmosphere Model Version 5 (CAM5) using stable isotope ratios of water.

Journal of Advances in Modeling Earth Systems **9** (2): 949–977 DOI: 10.1002/2016MS000839

Pope VD, Gallani ML, Rowntree PR, Stratton RA. 2000. The impact of new physical parametrizations in the Hadley Centre climate model: HadAM3. *Climate Dynamics* **16** (2–3): 123–146 DOI: 10.1007/s003820050009

Rindsberger M, Magaritz M, Carmi I, Gilad D. 1983. The relation between air mass trajectories and the water isotope composition of rain in the Mediterranean Sea area. *Geophysical Research Letters* **10** (1): 43–46 DOI: 10.1029/GL010i001p00043

Risi C, Bony S, Vimeux F. 2008. Influence of convective processes on the isotopic composition (δ^{18}O and δD) of precipitation and water vapor in the tropics: 2. Physical interpretation of the amount effect. *Journal of Geophysical Research* **113** (D19) DOI: 10.1029/2008JD009943

Risi C, Bony S, Vimeux F, Jouzel J. 2010. Water-stable isotopes in the LMDZ4 general circulation model: Model evaluation for present-day and past climates and applications to climatic interpretations of tropical isotopic records. *Journal of Geophysical Research* **115** (D12) DOI: 10.1029/2009JD013255

Risi C, Noone D, Worden J, Frankenberg C, Stiller G, Kiefer M, Funke B, Walker K, Bernath P, Schneider M, et al. 2012a. Process-evaluation of tropospheric humidity simulated by general circulation models using water vapor isotopic observations: 2. Using isotopic diagnostics to understand the mid and upper tropospheric moist bias in the tropics and subtropics. *Journal of Geophysical Research: Atmospheres* **117** (D5): n/a-n/a DOI: 10.1029/2011JD016623

Risi C, Noone D, Worden J, Frankenberg C, Stiller G, Kiefer M, Funke B, Walker K, Bernath P, Schneider M, et al. 2012b. Process-evaluation of tropospheric humidity simulated by general circulation models using water vapor isotopologues: 1. Comparison between models and observations. *Journal of Geophysical Research: Atmospheres* **117** (D5): n/a-n/a DOI: 10.1029/2011JD016621

Roeckner E, Bäuml G, Bonaventura L, Brokopf R, Esch M, Giorgetta M, Hagemann S, Kornblueh L, Schlese U, Schulzweida U, et al. 2003. The Atmospheric General Circulation Model ECHAM5. Model Description 349. Max-Planck-Institut für Meteorologie, Hamburg.

Rozanski K, Araguás-Araguás L, Gonfiantini R. 1993. Isotopic Patterns in Modern Global Precipitation. In *Geophysical Monograph Series*, Swart PK, , Lohmann KC, , Mckenzie J, , Savin S (eds).American Geophysical Union: Washington, D. C.; 1–36. DOI: 10.1029/GM078p0001

Ruosteenoja K, Jylhä K, Räisänen J, Mäkelä A. 2017. Surface air relative humidities spuriously exceeding 100% in CMIP5 model output and their impact on future projections. *Journal of Geophysical Research: Atmospheres* **122** (18): 9557–9568 DOI: 10.1002/2017JD026909

Sanderson BM, Wehner MF, Knutti R. 2017. Skill and independence weighting for multi-model assessments. *Geoscientific Model Development* **10**: 2379–2395 DOI: 10.5194/gmd-10-2379-2017

Schmidt GA, LeGrande AN, Hoffmann G. 2007. Water isotope expressions of intrinsic and forced variability in a coupled ocean-atmosphere model. *Journal of Geophysical Research: Atmospheres* **112** (D10) DOI: 10.1029/2006JD007781

Schmidt GA, Ruedy R, Hansen JE, Aleinov I, Bell N, Bauer M, Bauer S, Cairns B, Canuto V, Cheng Y, et al. 2006. Present-Day Atmospheric Simulations Using GISS ModelE: Comparison to In Situ, Satellite, and Reanalysis Data. *Journal of Climate* **19** (2): 153–192 DOI: 10.1175/JCLI3612.1

Schoch-Fischer H, Rozanski K, Jacob H, Sonntag C, Jouzel J, Östlund G, Geyh MA. 1984. Hydrometeorological factors controlling the time variation of D, 18O, and 3H in atmospheric water vapour and precipitation in the northern westwind belt. In *Isotope Hydrology 1983: Proceedings of a Symposium,* Vienna, Austria.

Siegenthaler U, Oeschger H. 1980. Correlation of ^{18}O in precipitation with temperature and altitude. *Nature* **285** (5763): 314

Soderberg K, Good SP, Wang L, Caylor K. 2012. Stable Isotopes of Water Vapor in the Vadose Zone: A Review of Measurement and Modeling Techniques. *Vadose Zone Journal* **11** (3): 0 DOI: 10.2136/vzj2011.0165

Steiger NJ, Steig EJ, Dee SG, Roe GH, Hakim GJ. 2017. Climate reconstruction using data assimilation of water isotope ratios from ice cores. *Journal of Geophysical Research: Atmospheres* **122** (3): 1545–1568 DOI: 10.1002/2016JD026011

[dataset]Steiger, NJ. (2018). Historical climate model output of ECHAM5-wiso from 1871-2011 at T106 resolution [Data set]. Zenodo. http://doi.org/10.5281/zenodo.1249604

Stewart MK. 1975. Stable isotope fractionation due to evaporation and isotopic exchange of falling waterdrops: Applications to atmospheric processes and evaporation of lakes. *Journal of Geophysical Research* **80** (9): 1133–1146 DOI: 10.1029/JC080i009p01133

[dataset]Stable Water Isotope Intercomparison Group, Phase 2. Hosted by NASA Goddard Institute for Space Studies. https://data.nasa.giss.gov/swing2.

Thorpe AS, Barnett DT, Elmendorf SC, Hinckley E-LS, Hoekman D, Jones KD, LeVan KE, Meier CL, Stanish LF, Thibault KM. 2016. Introduction to the sampling designs of the National Ecological Observatory Network Terrestrial Observation System. *Ecosphere* **7** (12): e01627 DOI: 10.1002/ecs2.1627

Tindall JC, Valdes PJ, Sime LC. 2009. Stable water isotopes in HadCM3: Isotopic signature of El Niño–Southern Oscillation and the tropical amount effect. *Journal of Geophysical Research* **114** (D4) DOI: 10.1029/2008JD010825

Tremoy G, Vimeux F, Mayaki S, Souley I, Cattani O, Risi C, Favreau G, Oi M. 2012. A 1-year long $\delta^{18}O$ record of water vapor in Niamey (Niger) reveals insightful atmospheric processes at different timescales. *Geophysical Research Letters* **39** (8): n/a-n/a DOI: 10.1029/2012GL051298

Trenberth KE, Zhang Y. 2018. How Often Does It Really Rain? *Bulletin of the American Meteorological Society* **99** (2): 289–298 DOI: 10.1175/BAMS-D-17-0107.1

Vimeux F, Gallaire R, Bony S, Hoffmann G, Chiang J. 2005. What are the climate controls on δD in precipitation in the Zongo Valley (Bolivia)? Implications for the Illimani ice core interpretation. *Earth and Planetary Science Letters* **240** (2): 205–220 DOI: 10.1016/j.epsl.2005.09.031

Wei Z, Lee X, Aemisegger F, Benetti M, Berkelhammer M, Casado M, Caylor K, Christner E, Dyroff C, García O, et al. 2019. A global database of water vapor isotopes measured with high temporal resolution infrared laser spectroscopy. *Scientific Data* **6**: 180302 DOI: 10.1038/sdata.2018.302

Welp LR, Lee X, Griffis TJ, Wen X-F, Xiao W, Li S, Sun X, Hu Z, Val Martin M, Huang J. 2012. A meta-analysis of water vapor deuterium-excess in the midlatitude atmospheric surface layer. *Global Biogeochemical Cycles* **26** (3) DOI: 10.1029/2011GB004246

Welp LR, Lee X, Kim K, Griffis TJ, Billmark KA, Baker JM. 2008. δ^{18}O of water vapour, evapotranspiration and the sites of leaf water evaporation in a soybean canopy. *Plant, Cell & Environment* **31** (9): 1214–1228 DOI: 10.1111/j.1365-3040.2008.01826.x

Wen X-F, Lee X, Sun X-M, Wang J-L, Hu Z-M, Li S-G, Yu G-R. 2012. Dew water isotopic ratios and their relationships to ecosystem water pools and fluxes in a cropland and a grassland in China. *Oecologia* **168** (2): 549–561

Werner M, Langebroek PM, Carlsen T, Herold M, Lohmann G. 2011. Stable water isotopes in the ECHAM5 general circulation model: Toward high-resolution isotope modeling on a global scale. *Journal of Geophysical Research* **116** (D15) DOI: 10.1029/2011JD015681

West JB, Sobek A, Ehleringer JR. 2008. A Simplified GIS Approach to Modeling Global Leaf Water Isoscapes. *PLoS ONE* **3** (6): e2447 DOI: 10.1371/journal.pone.0002447

Wong TE, Nusbaumer J, Noone DC. 2017. Evaluation of modeled land-atmosphere exchanges with a comprehensive water isotope fractionation scheme in version 4 of the Community Land Model. *Journal of Advances in Modeling Earth Systems* **9** (2): 978–1001 DOI: 10.1002/2016MS000842

Worden J, Kulawik S, Frankenberg C, Payne V, Bowman K, Cady-Peirara K, Wecht K, Lee J-E, Noone D. 2012. Profiles of CH_4, HDO, H_2O, and N_2O with improved lower tropospheric vertical resolution from Aura TES radiances. *Atmospheric Measurement Techniques* **5** (2): 397–411 DOI: 10.5194/amt-5-397-2012

Yoshimura K, Kanamitsu M, Noone D, Oki T. 2008. Historical isotope simulation using Reanalysis atmospheric data. *Journal of Geophysical Research* **113** (D19) DOI: 10.1029/2008JD010074

Tables

Table 1. Summary of models used in this study.

Model Name	Native Resolution	Isotopic variables	Meteorological Variables	Model Reference	Isotopic Reference
CAM2	T42 (~2.8x2.8°)	Precipitation, vapor, and evaporation flux	T, Q, U, V, Ω, P_{sfc}	(Collins *et al.*, 2002)	(Lee *et al.*, 2007)
CAM5	0.9x1.25°	Precipitation, vapor, and evaporation flux	T, Q, U, V, Ω, P_{sfc}	(Neale *et al.*, 2010)	(Nusbaumer *et al.*, 2017; Wong *et al.*, 2017)
ECHAM5	T106 (~1.1x1.1°)	Precipitation and vapor only	T_{sfc}, Q_{sfc}, U, V, P_{sfc}	(Roeckner *et al.*, 2003)	(Werner *et al.*, 2011; Steiger *et al.*, 2017)
GISS ModelE	2x2.5°	Land evaporation, global precipitation and vapor	T, Q, U, V, P_{sfc}	(Schmidt *et al.*, 2006)	(Schmidt *et al.*, 2007)
HadAM3	2.5x3.75°	Precipitation, vapor, and evaporation flux	T, Q, U, V	(Pope *et al.*, 2000)	(Tindall *et al.*, 2009)
isoGSM	2.5x2.5°	Precipitation, vapor, and evaporation flux	T, Q, U, V, Ω, P_{sfc}	(Kanamitsu *et al.*, 2002)	(Yoshimura *et al.*, 2008)
LMDZ4	2.5x3.75°	Precipitation and vapor only	T, Q, U, V, Ω, P_{sfc}	(Hourdin *et al.*, 2006)	(Risi *et al.*, 2010)
MIROC	T42 (~2.8x2.8°)	Precipitation, vapor, and evaporation flux	T, Q, U, V, Ω	(K-1 model developers)	(Kurita *et al.*, 2011)

Figure Captions

Figure 1. Annual average $\Delta(\delta^2H_{atm})$ values for historical simulations spanning 1980-2000 for (a) CAM2, (b) CAM5, (c) ECHAM5, (d) GISS ModelE, (e) HadAM3, (f) isoGSM, (g) LMDZ4, and (h) MIROC. The final two panels provide an equal-weight ensemble mean (i) and standard deviation (j) for $\Delta(\delta^2H_{atm})$.

Figure 2. Zonal average $\Delta(\delta^2H_{atm})$ values for DJF (a and b) and JJA (c and d) for each model in the ensemble, with the ensemble average shown as a solid black line. Extreme values south of 70°S are truncated to better show variations between other latitudes. The left column shows all grid cells (land and ocean, a and c) while the right column shows only land grid cells (b and d).

Figure 3. Box-and-whisker plots showing the distribution of $\Delta(\delta_{atm})$ values across the model ensemble, with values from Antarctica excluded. Distributions for land and ocean grid cells are shown in the top row (a and b), while distributions for land grid cells only are shown in the bottom row (c and d). The left column shows $\Delta(\delta^2H_{atm})$ while the right column shows $\Delta(\delta^{18}O_{atm})$. Boxes correspond to the 25th-75th percentile with the median indicated with a solid black line, while the whiskers extend to the 2.5th and 97.5th percentiles and indicate the central 95% of the data.

Figure 4. Relationships between $\Delta(\delta^2H_{atm})$ and meteorological variables derived from the model ensemble. (a) Evaporation (mm/day) against precipitation (mm/day) colored by $\Delta(\delta^2H_{atm})$, with the 1:1 relationship between evaporation and precipitation shown as a dashed black line. (b) 500 hPa vertical pressure velocity (hPa) against precipitation colored by $\Delta(\delta^2H_{atm})$. (c) $\Delta(\delta^2H_{atm})$ (‰

VSMOW) plotted against precipitation (mm/day), colored by the precipitation to evaporation ratio.

Figure 5. Modeled atmospheric vapor and vapor in equilibrium with precipitation in relation to isotopic models. (a) δ^2H of annual ensemble mean vapor (δ^2H_v) and (b) δ^2H of vapor in equilibrium ($\delta^2H_{v,e}$) with annual ensemble mean precipitation against specific humidity (*q,* mmol/mol). In (a) and (b), box-model predictions representing air-mass mixing along an equator-to-pole gradient (red line) and Rayleigh distillation (black line) are shown. (c) Distributions showing the deviation of δ^2H_v and $\delta^2H_{v,e}$ from air-mass mixing and Rayleigh distillation model predictions.

Figure 6. Zonal average $\Delta(\delta^2H_{diseq})$ over land and its incorporation into evaporating waters. (a) Zonal annual average $\Delta(\delta^2H_{diseq})$ (b) zonal annual average relative humidity, and (c) zonal annual average $\Delta(\delta^2H_L)$ for each model. HadAM3 is missing from panels (b) and (c) as this model did not provide variables required to estimate relative humidity.

Figure 7. Comparison of δ^2H_v to $\delta^2H_{v,e}$ when $\delta^2H_{v,e}$ is calculated with respect to (a) long-term annual average precipitation isotope ratios, and (b) monthly precipitation isotope ratios. Distributions of δ^2H_v–$\delta^2H_{v,e}$ for each of these assumptions is shown in (c), with box plots indicating the central 50% (boxes) and 95% (whiskers) of the data. A 1:1 line is shown in (a) and (b) for reference.

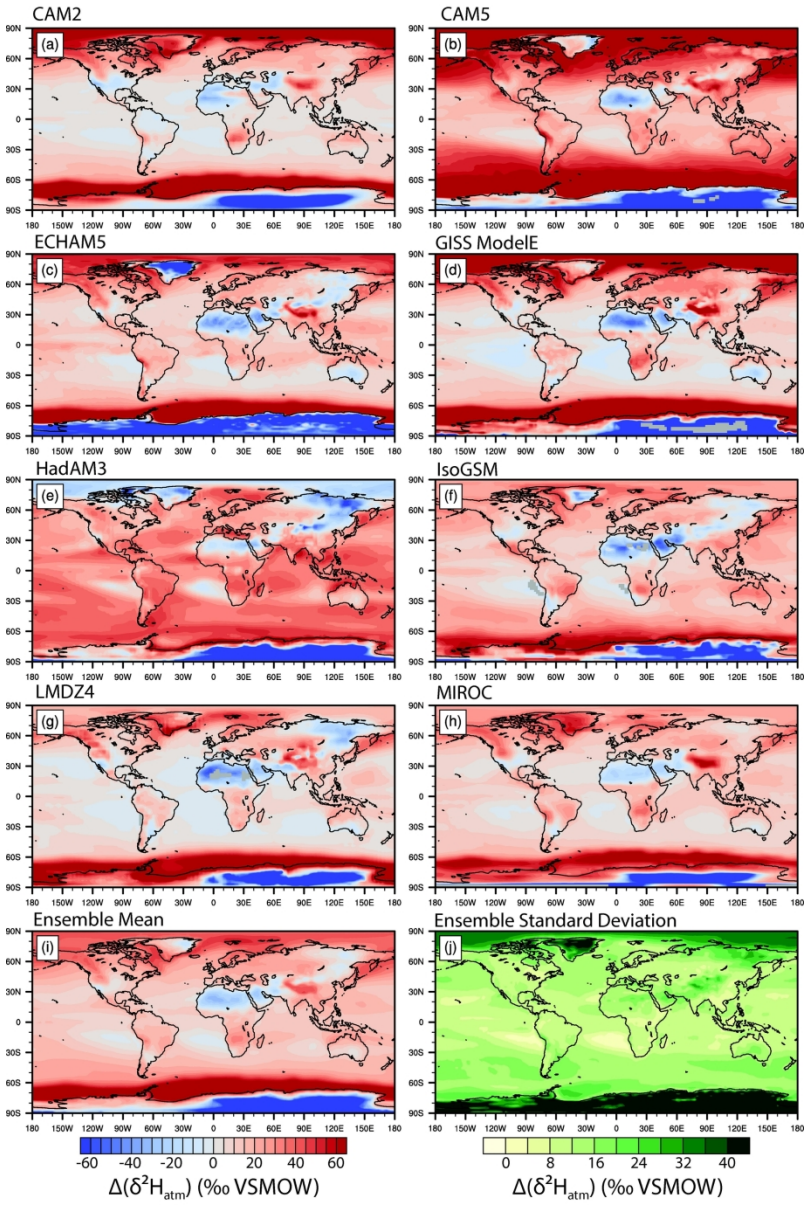

Figure 1. Annual average $\Delta(\delta^2H_{atm})$ values for historical simulations spanning 1980-2000 for (a) CAM2, (b) CAM5, (c) ECHAM5, (d) GISS ModelE, (e) HadAM3, (f) isoGSM, (g) LMDZ4, and (h) MIROC. The final two panels provide an equal-weight ensemble mean (i) and standard deviation (j) for $\Delta(\delta^2H_{atm})$.

171x257mm (300 x 300 DPI)

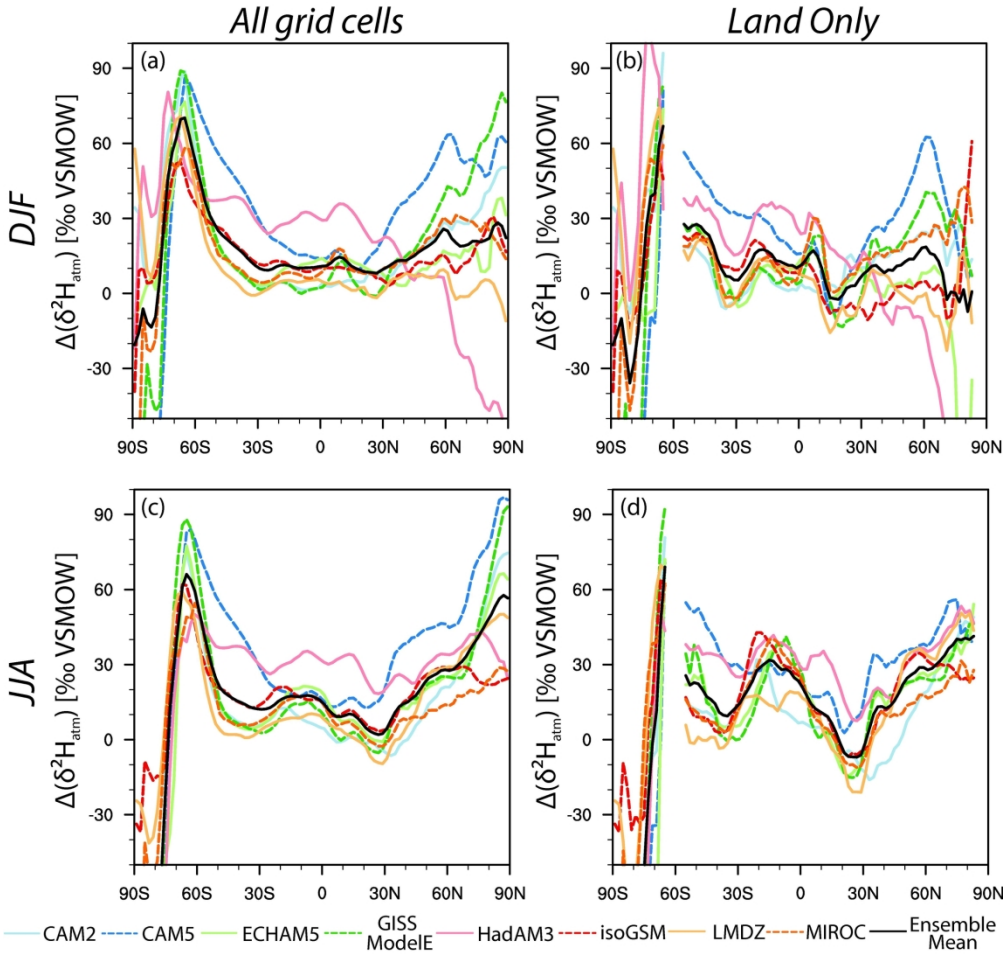

Figure 2. Zonal average $\Delta(\delta^2H_{atm})$ values for DJF (a and b) and JJA (c and d) for each model in the ensemble, with the ensemble average shown as a solid black line. Extreme values south of 70°S are truncated to better show variations between other latitudes. The left column shows all grid cells (land and ocean, a and c) while the right column shows only land grid cells (b and d).

199x189mm (300 x 300 DPI)

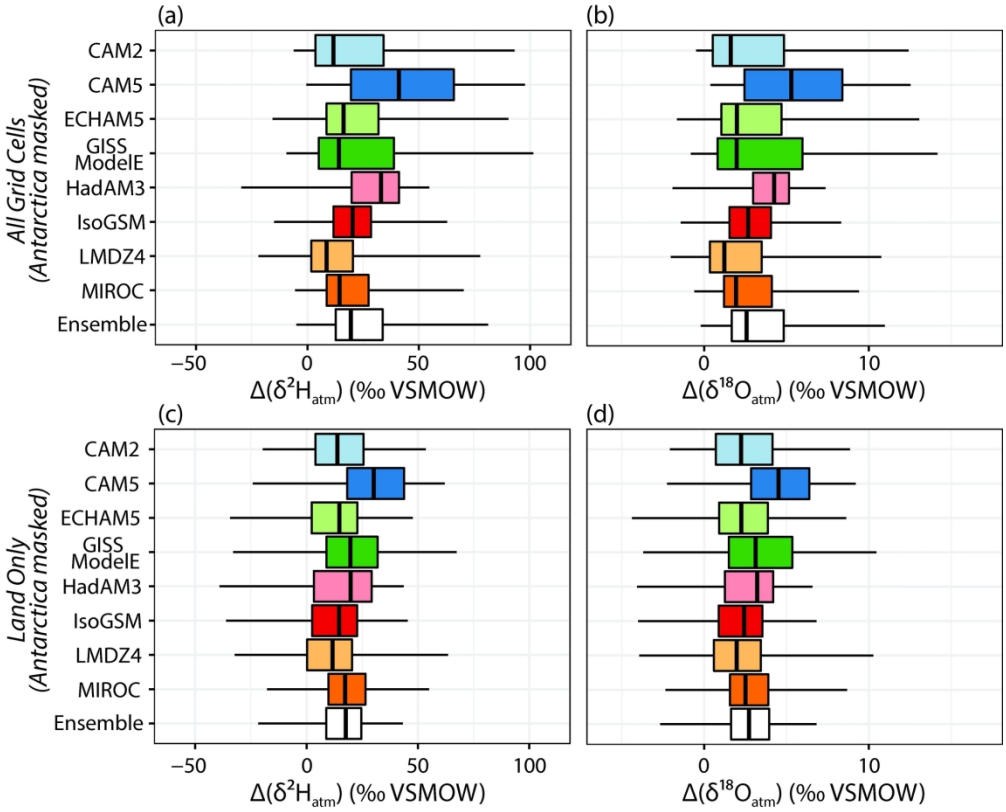

Figure 3. Box-and-whisker plots showing the distribution of $\Delta(\delta_{atm})$ values across the model ensemble, with values from Antarctica excluded. Distributions for land and ocean grid cells are shown in the top row (a and b), while distributions for land grid cells only are shown in the bottom row (c and d). The left column shows $\Delta(\delta^2H_{atm})$ while the right column shows $\Delta(\delta^{18}O_{atm})$. Boxes correspond to the 25th-75th percentile with the median indicated with a solid black line, while the whiskers extend to the 2.5th and 97.5th percentiles and indicate the central 95% of the data.

192x155mm (300 x 300 DPI)

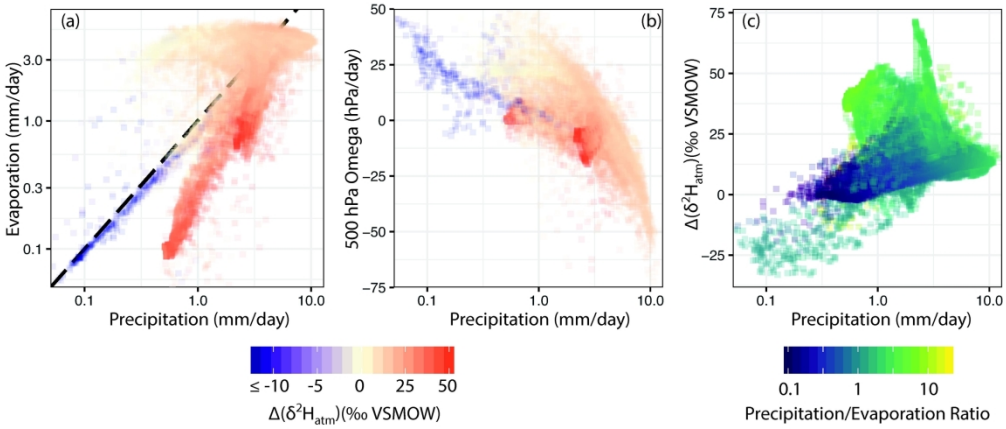

Figure 4. Relationships between $\Delta(\delta^2H_{atm})$ and meteorological variables derived from the model ensemble. (a) Evaporation (mm/day) against precipitation (mm/day) colored by $\Delta(\delta^2H_{atm})$, with the 1:1 relationship between evaporation and precipitation shown as a dashed black line. (b) 500 hPa vertical pressure velocity (ω, hPa) against precipitation colored by $\Delta(\delta^2H_{atm})$. (c) $\Delta(\delta^2H_{atm})$ (‰ VSMOW) plotted against precipitation (mm/day), colored by the precipitation to evaporation ratio.

224x96mm (300 x 300 DPI)

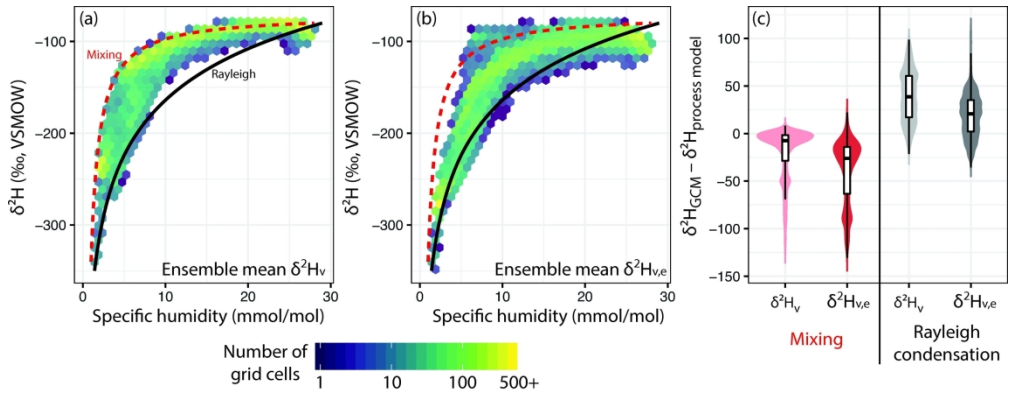

Figure 5. Modeled atmospheric vapor and vapor in equilibrium with precipitation in relation to isotopic models. (a) δ^2H of annual ensemble mean vapor (δ^2H_v) and (b) δ^2H of vapor in equilibrium ($\delta^2H_{v,e}$) with annual ensemble mean precipitation against specific humidity (q, mmol/mol). In (a) and (b), model predictions representing air-mass mixing along an equator-to-pole gradient (red line) and Rayleigh distillation (black line) are shown. (c) Distributions showing the deviation of δ^2H_v and $\delta^2H_{v,e}$ from air-mass mixing and Rayleigh distillation model predictions.

225x87mm (300 x 300 DPI)

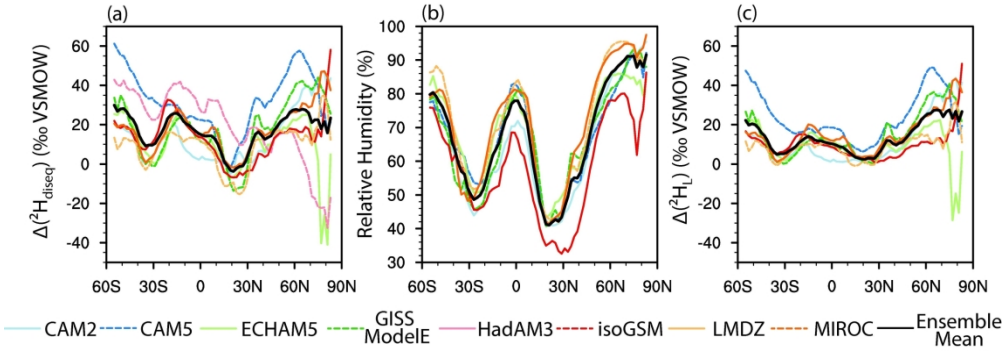

Figure 6. Zonal average $\Delta(\delta^2H_{diseq})$ over land and its incorporation into evaporating waters. (a) Zonal annual average $\Delta(\delta^2H_{diseq})$ (b) zonal annual average relative humidity, and (c) zonal annual average $\Delta(\delta^2H_L)$ for each model. HadAM3 is missing from panels (b) and (c) as this model did not provide variables required to estimate relative humidity.

200x69mm (300 x 300 DPI)

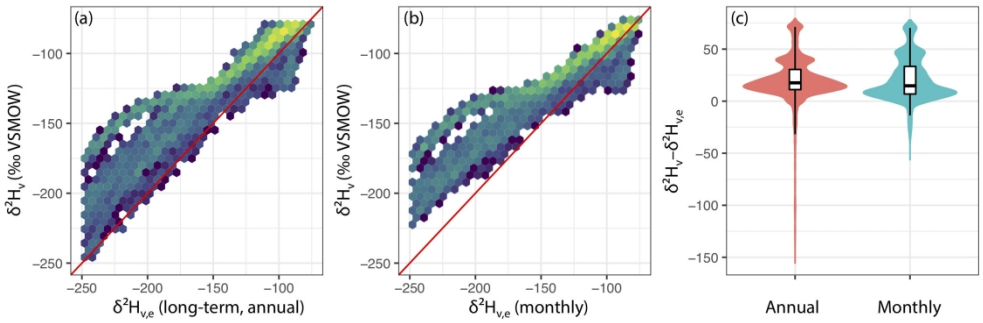

Figure 7. Comparison of δ^2H_v to $\delta^2H_{v,e}$ when $\delta^2H_{v,e}$ is calculated with respect to (a) long-term annual average precipitation isotope ratios, and (b) monthly precipitation isotope ratios. Distributions of δ^2H_v–$\delta^2H_{v,e}$ for each of these assumptions is shown in (c), with box plots indicating the central 50% (boxes) and 95% (whiskers) of the data. A 1:1 line is shown in (a) and (b) for reference.

Supporting information for "Biased estimates of the isotope ratios of steady-state evaporation from the assumption of equilibrium between vapor and precipitation"

Richard P. Fiorella[1], Jason B. West[2], Gabriel J. Bowen[1,3]

1. Department of Geology and Geophysics, University of Utah, Salt Lake City, UT
2. Department of Ecosystem Science and Management, Texas A&M University, College Station, TX
3. Global Change and Sustainability Center, University of Utah, Salt Lake City, UT

This supporting information document contains eight supplementary figures.

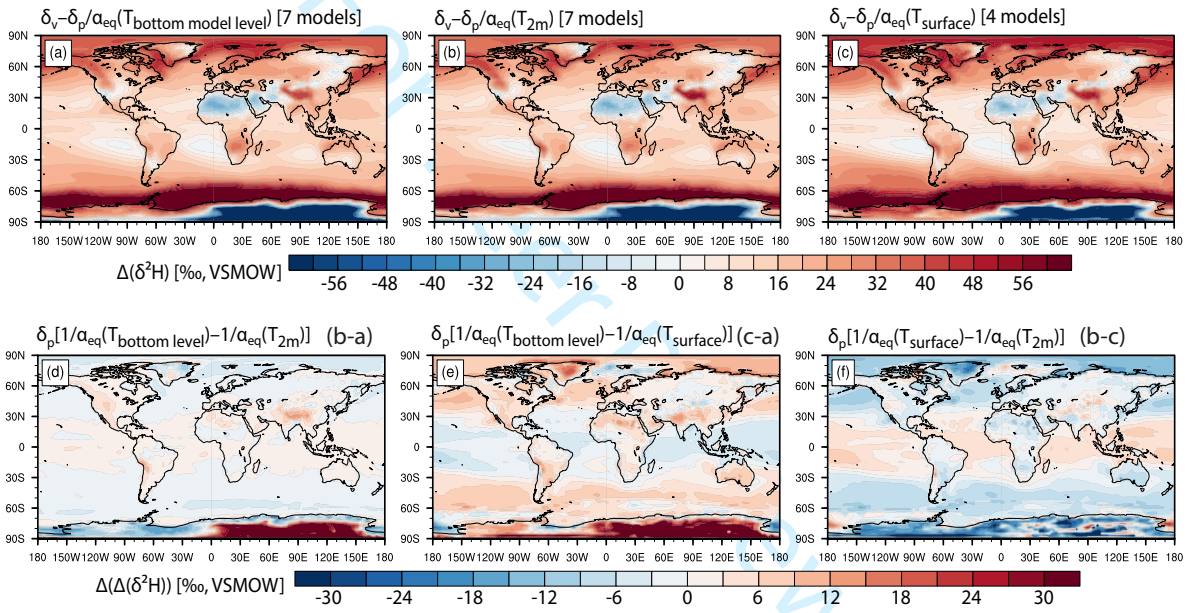

Figure S1. Comparison of $\Delta(\delta^2H_{atm})$ values calculated using fractionation factors calculated from (a) lowest model level temperature, (b) 2-meter temperature, or (c) surface skin temperatures. Differences between pairs of $\Delta(\delta^2H_{atm})$ values are shown in the bottom row: (d) $\Delta(\delta^2H_{atm})$ using bottom level temperatures compared to 2-meter temperatures, (e) bottom level temperatures compared to surface temperatures, and (f) surface temperatures compared to 2-meter temperatures.

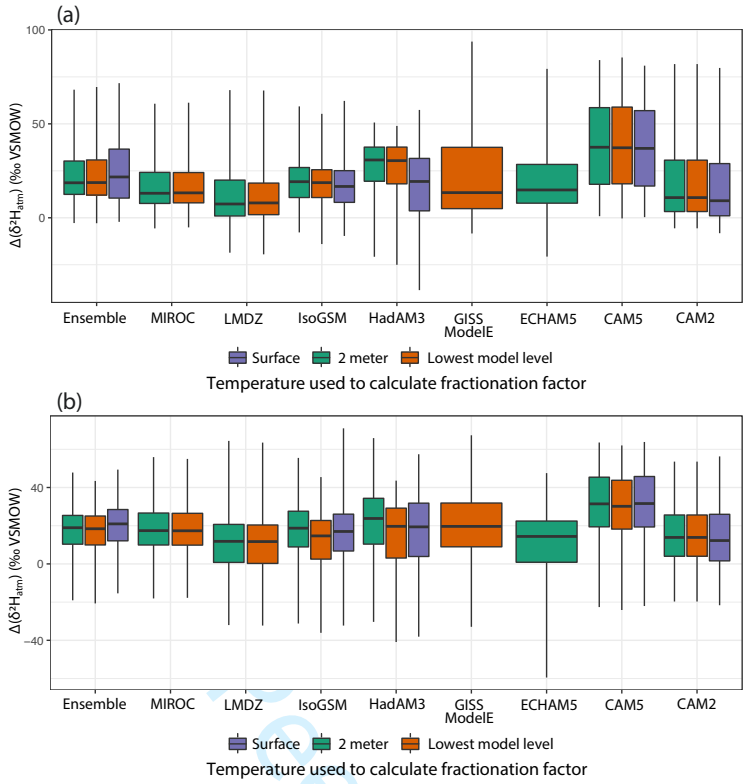

Figure S2. Global distribution of $\Delta(\delta^2H_{atm})$ values for all grid cells except Antarctica (a) and only land grid cells (b), calculated using fractionation factors calculated from lowest model level temperature (orange), 2-meter temperature (green), or surface skin temperatures (purple).

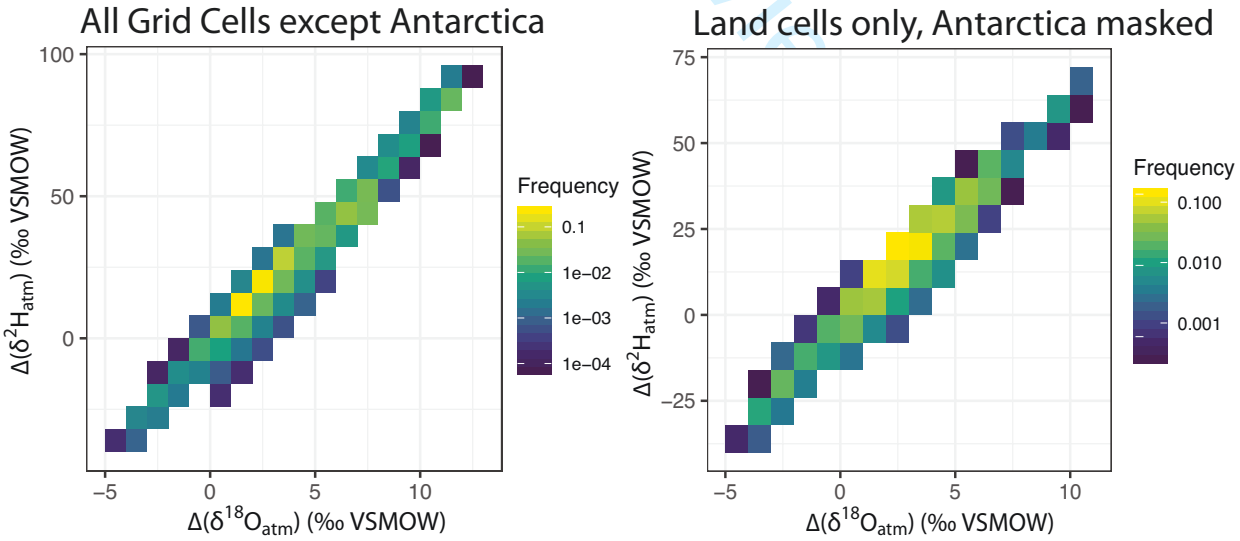

Figure S3. Relationship between $\Delta(\delta^2H_{atm})$ and $\Delta(\delta^{18}O_{atm})$ for all cells (a) and land cells only (b), with cells from Antarctica masked. Data are plotted showing the frequency of grid cells, placed into 8‰ (for $\Delta(\delta^2H_{atm})$) by 1‰ (for $\Delta(\delta^{18}O_{atm})$) boxes.

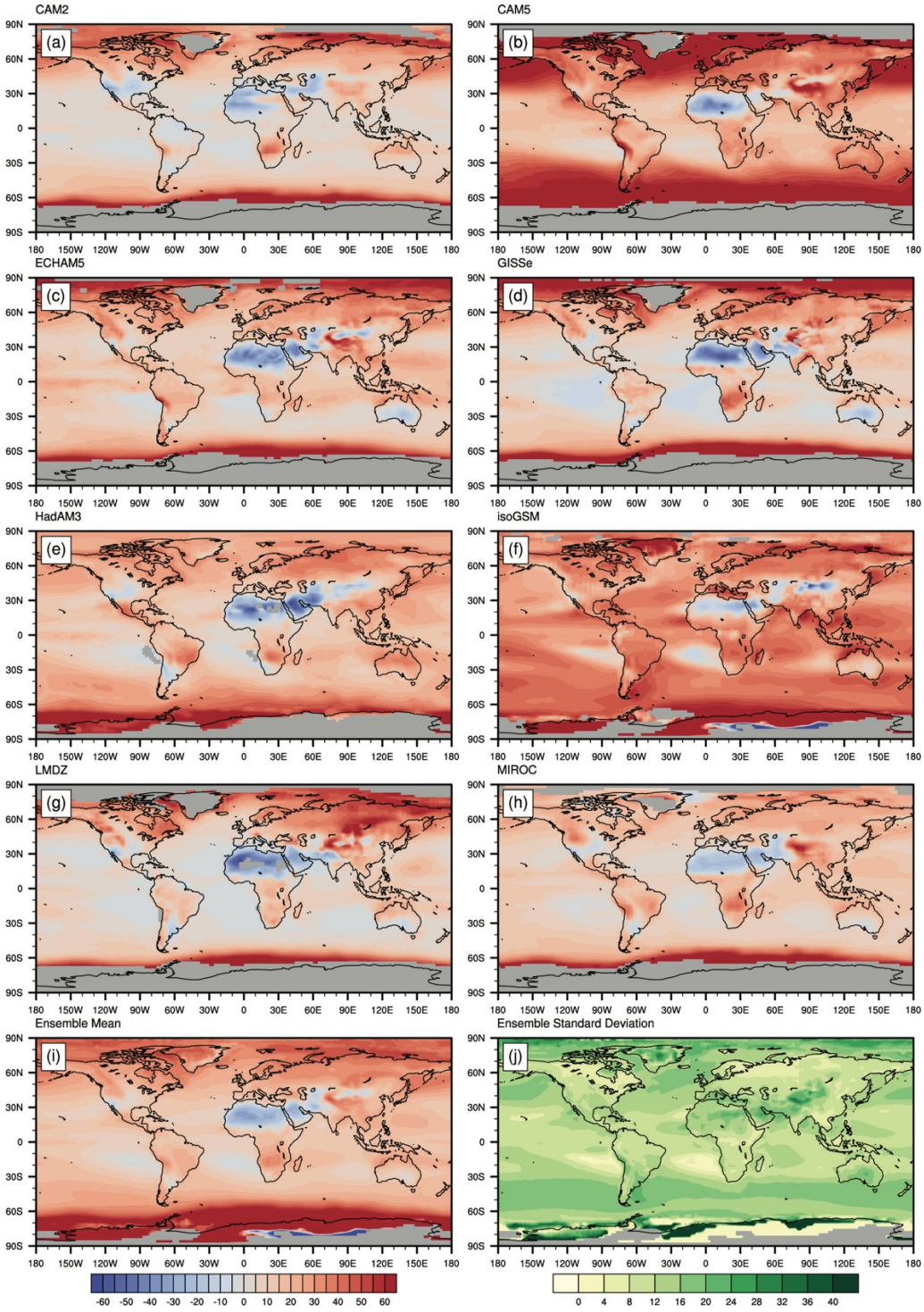

Figure S4. Average $\Delta(\delta^2H_{atm})$ values for historical simulations spanning 1980-2000, including only months with T > 0°C, for (a) CAM2, (b) CAM5, (c) ECHAM5, (d) GISS ModelE, (e) HadAM3, (f) isoGSM, (g) LMDZ4, and (h) MIROC. The final two panels provide an equal-weight ensemble mean (i) and standard deviation (j) for $\Delta(\delta^2H_{atm})$. Gray areas indicate no months were had T > 0°C.

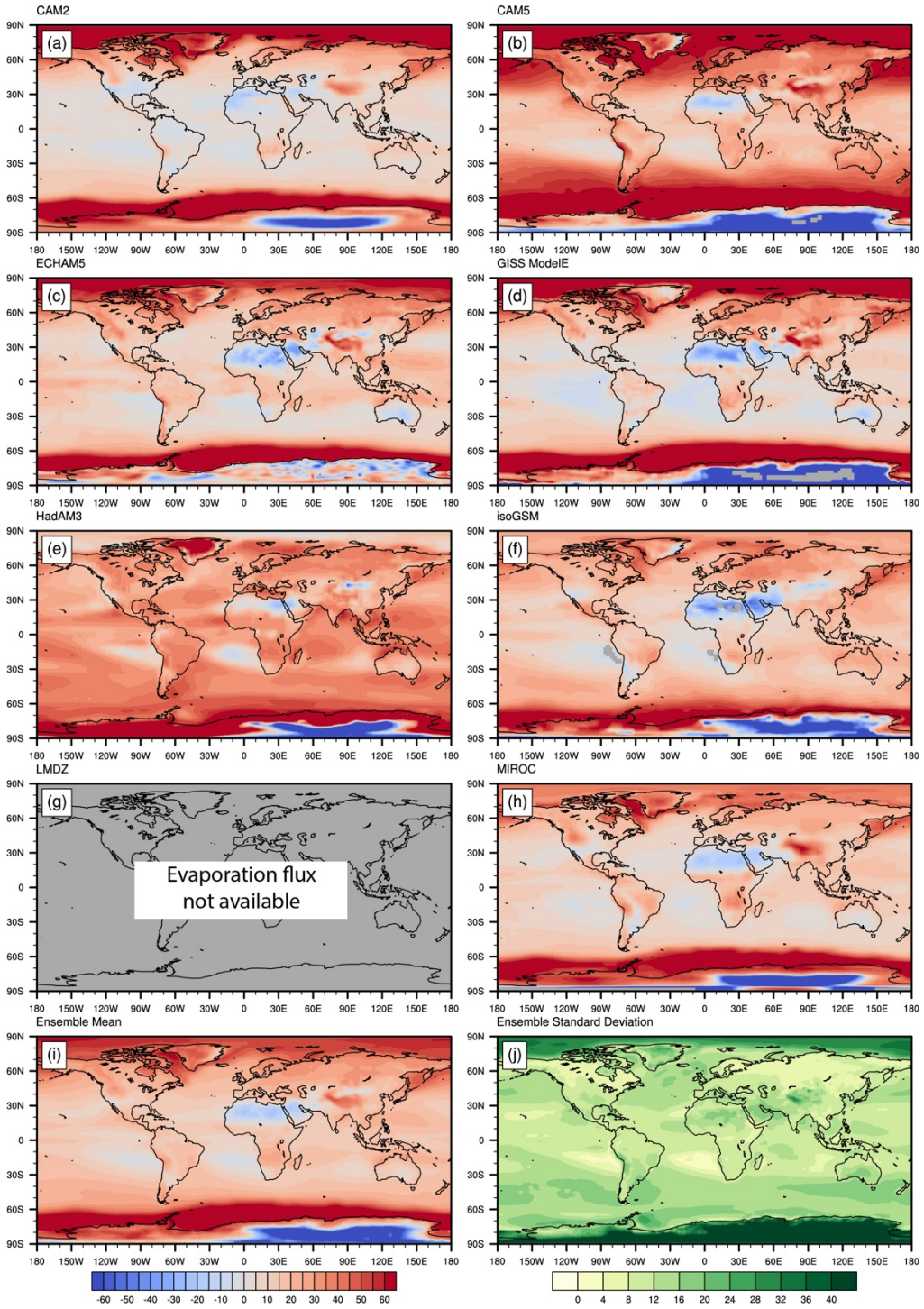

Figure S5. Annual average $\Delta(\delta^2H_{atm})$ values for historical simulations spanning 1980-2000, weighted by the monthly evaporation flux, for (a) CAM2, (b) CAM5, (c) ECHAM5, (d) GISS ModelE, (e) HadAM3, (f) isoGSM, (g) LMDZ4, and (h) MIROC. The final two panels provide an equal-weight ensemble mean (i) and standard deviation (j) for $\Delta(\delta^2H_{atm})$. No data are provided for LMDZ, as the SWING2 archive did not store evaporation fluxes for this model.

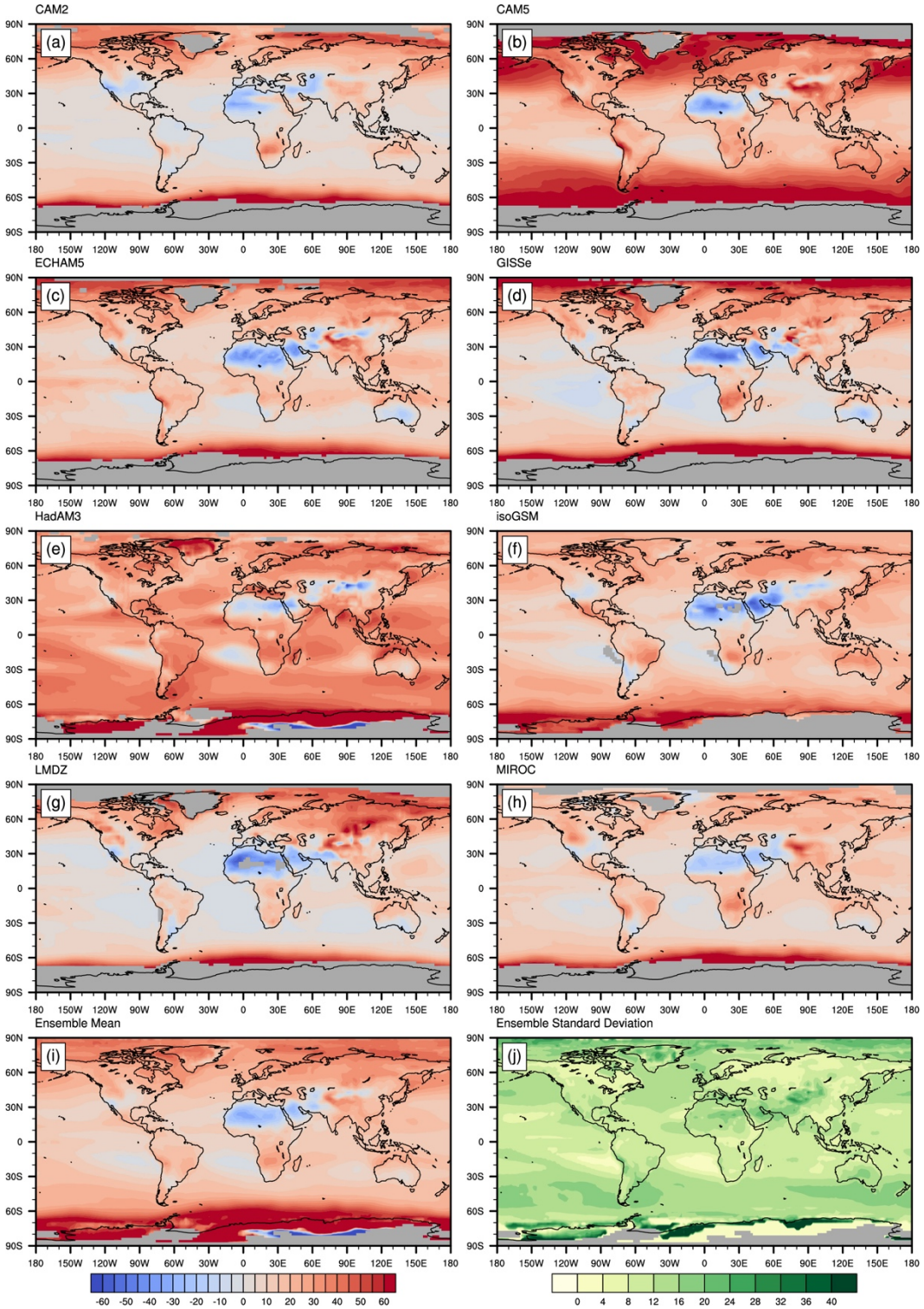

Figure S6. Annual average $\Delta(\delta^2H_{atm})$ values for historical simulations spanning 1980-2000, weighted by the monthly precipitation flux, for (a) CAM2, (b) CAM5, (c) ECHAM5, (d) GISS ModelE, (e) HadAM3, (f) isoGSM, (g) LMDZ4, and (h) MIROC. The final two panels provide an equal-weight ensemble mean (i) and standard deviation (j) for $\Delta(\delta^2H_{atm})$.

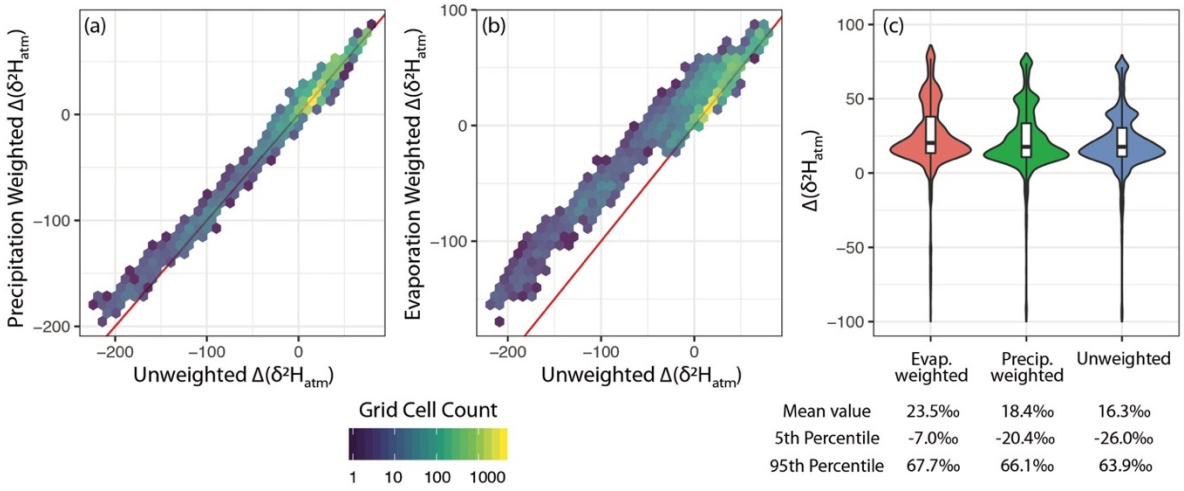

Figure S7. Comparison of flux-weighting assumptions to estimates of $\Delta(\delta^2H_{atm})$: (a) precipitation-weighted $\Delta(\delta^2H_{atm})$ against unweighted $\Delta(\delta^2H_{atm})$; (b) evaporation-weighted $\Delta(\delta^2H_{atm})$ against unweighted $\Delta(\delta^2H_{atm})$; (c) comparison of the distributions of all three assumptions.

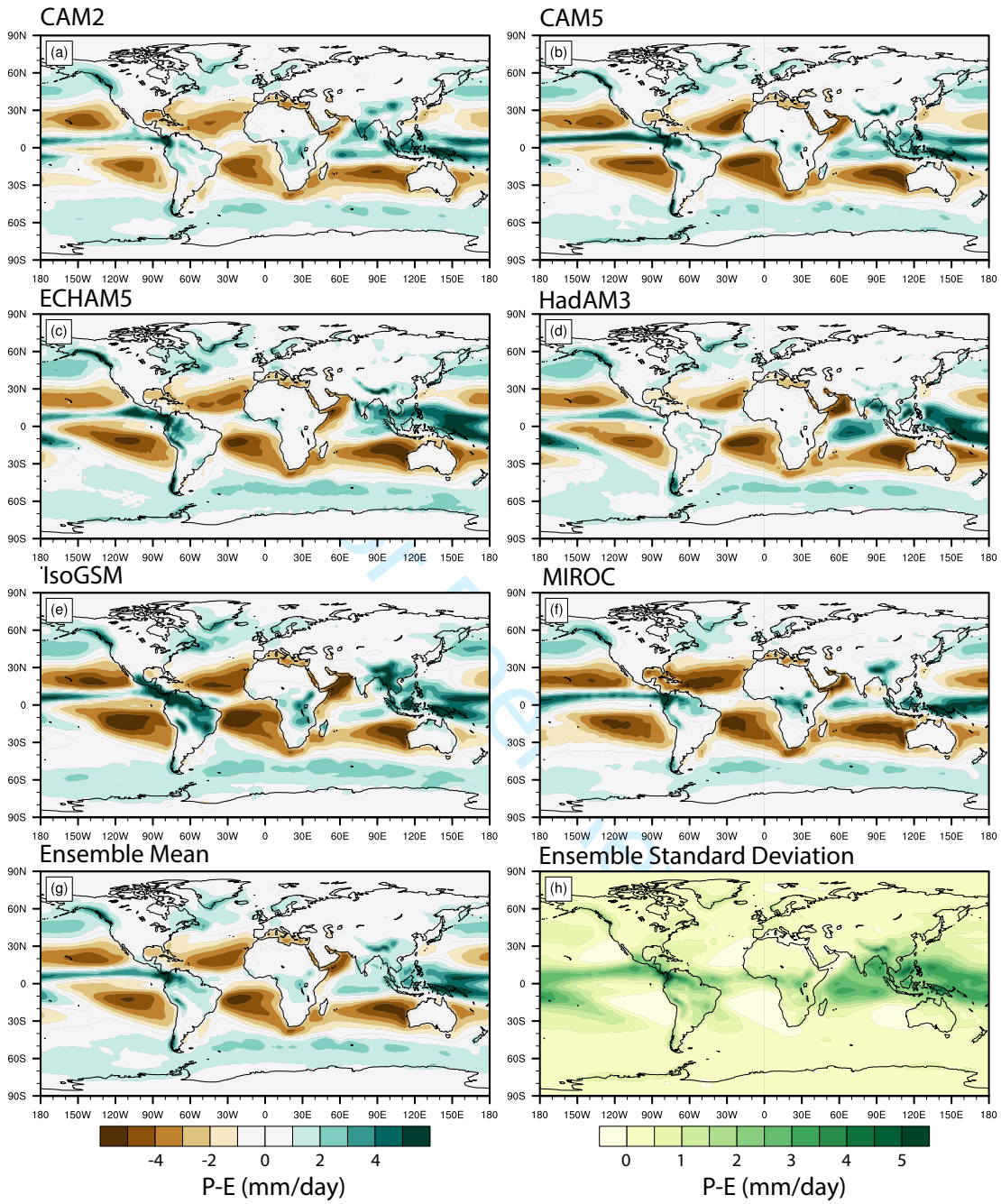

Figure S8. Maps of long-term annual average precipitation minus evaporation (P-E, mm/day) across the model ensemble (a-f), ensemble mean P-E (g) and standard deviation (h). Large standard deviations are small except in the tropics; large tropical variation arises from differences in the ITCZ position between models. GISS ModelE and LMDZ4 are excluded from this figure as evaporative fluxes were not archived for these models.

Accurate modeling of water isotopes during evaporation requires an estimate of the isotope ratio of atmospheric water vapor and is often assumed to be in isotopic equilibrium with precipitation. We test this assumption using an ensemble of isotope-enabled climate models. We find this assumption works well at low latitudes, but that moisture transport causes vapor isotope ratios to be higher than equilibrium-predicted values at high latitudes.

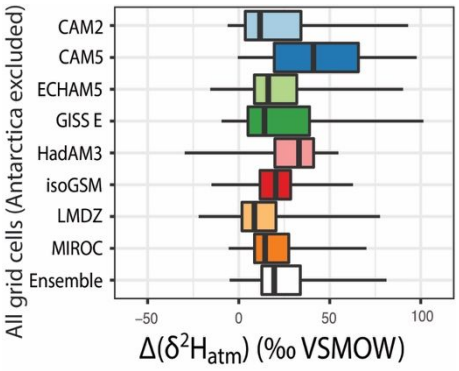

Biased estimates of the isotope ratios of steady-state evaporation from the assumption of equilibrium between vapor and precipitation

Richard P. Fiorella*, Jason B. West, Gabriel J. Bowen